IOP Publishing | Institute of Physics and Engineering in Medicine Physics in Medicine & Biology

Phys. Med. Biol. **61** (2016) 3443–3471 doi:10.1088/0031-9155/61/9/3443

Impact of time-of-flight on indirect 3D and direct 4D parametric image reconstruction in the presence of inconsistent dynamic PET data

F A Kotasidis[1,2], A Mehranian[1] and H Zaidi[1,3,4]

[1] Division of Nuclear Medicine and Molecular Imaging, Geneva University Hospital, CH-1211, Geneva, Switzerland
[2] Wolfson Molecular Imaging Centre, MAHSC, University of Manchester, M20 3LJ, Manchester, UK
[3] Geneva Neuroscience Centre, Geneva University, CH-1205 Geneva, Switzerland
[4] Department of Nuclear Medicine and Molecular Imaging, University of Groningen, University Medical Center Groningen, 9700 RB, Groningen, The Netherlands

E-mail: fotis.kotasidis@unige.ch

Received 9 December 2015, revised 29 February 2016
Accepted for publication 16 March 2016
Published 6 April 2016

Abstract

Kinetic parameter estimation in dynamic PET suffers from reduced accuracy and precision when parametric maps are estimated using kinetic modelling following image reconstruction of the dynamic data. Direct approaches to parameter estimation attempt to directly estimate the kinetic parameters from the measured dynamic data within a unified framework. Such image reconstruction methods have been shown to generate parametric maps of improved precision and accuracy in dynamic PET. However, due to the interleaving between the tomographic and kinetic modelling steps, any tomographic or kinetic modelling errors in certain regions or frames, tend to spatially or temporally propagate. This results in biased kinetic parameters and thus limits the benefits of such direct methods. Kinetic modelling errors originate from the inability to construct a common single kinetic model for the entire field-of-view, and such errors in erroneously modelled regions could spatially propagate. Adaptive models have been used within 4D image reconstruction to mitigate the problem, though they are complex and difficult to optimize. Tomographic errors in dynamic imaging on the other hand, can originate from involuntary patient motion between dynamic frames, as well as from emission/transmission mismatch. Motion correction schemes can be used, however, if residual errors exist or motion correction is not included in the study protocol, errors in the affected dynamic frames could

potentially propagate either temporally, to other frames during the kinetic modelling step or spatially, during the tomographic step. In this work, we demonstrate a new strategy to minimize such error propagation in direct 4D image reconstruction, focusing on the tomographic step rather than the kinetic modelling step, by incorporating time-of-flight (TOF) within a direct 4D reconstruction framework. Using ever improving TOF resolutions (580 ps, 440 ps, 300 ps and 160 ps), we demonstrate that direct 4D TOF image reconstruction can substantially prevent kinetic parameter error propagation either from erroneous kinetic modelling, inter-frame motion or emission/transmission mismatch. Furthermore, we demonstrate the benefits of TOF in parameter estimation when conventional post-reconstruction (3D) methods are used and compare the potential improvements to direct 4D methods. Further improvements could possibly be achieved in the future by combining TOF direct 4D image reconstruction with adaptive kinetic models and inter-frame motion correction schemes.

Keywords: PET, time-of-flight, direct 4D reconstruction, parametric imaging

(Some figures may appear in colour only in the online journal)

1. Introduction

Pharmacokinetic modelling of dynamic PET data allows targeted physiological parameters to be derived. Compared to static imaging, dynamic imaging allows the time course of the activity distribution to be imaged and subsequently modelled following post-reconstruction kinetic analysis. When full compartmental analysis is used, maps of micro-parameters are derived, which represent different physiological parameters (Watabe *et al* 2006). However, dynamic data are particularly noisy owning to limited counting statistics and the need for increased temporal sampling, thus leading to estimated kinetic parameters of suboptimal accuracy and precision. 4D image reconstruction methods have been shown to improve parameter precision and accuracy. A number of 4D algorithms exist, with the direct 4D methods leading to direct estimation of parameters from the measured data in a unified framework (Reader and Verhaeghe 2014). Such algorithms are often specific to kinetic models and the nonlinear coupling of the kinetic parameters makes them often too complicated and slow to converge (Kamasak *et al* 2005, Jianhua *et al* 2012, Rakvongthai *et al* 2013). However, a number of algorithms lately attempt to separate the tomographic from the kinetic modelling step, thus allowing existing algorithms used for image reconstruction and kinetic modelling to be used within a 4D reconstruction framework (Wang and Qi 2009, 2012, Matthews *et al* 2010, Angelis *et al* 2011, Rahmim *et al* 2014, Gravel and Reader 2015). This is often achieved by interleaving the tomographic and kinetic modelling steps, which resembles the post-reconstruction methodology but converges to the 4D solution. Such approaches are easier to implement and allow a multitude of kinetic models to be used, opening the way for reconstructing dynamic data of new tracers using direct 4D methods. Direct 4D parameter estimation and its benefits have been extensively demonstrated in neuro-receptor and generally dynamic brain PET imaging. Nevertheless, so far their application to dynamic thoracic and abdominal imaging has been very limited (Kotasidis *et al* 2010, 2012a, Rahmim *et al* 2010, 2014). There are two issues arising when trying to directly estimate kinetic parameters in the body.

Firstly, using a single common kinetic model to describe the kinetics in the entire field-of-view (FOV) is challenging. In brain imaging, using a single model to describe the underlying temporal distribution of a given tracer is usually a valid approximation, with activity delivery through the carotid arteries and with a minimal differential delay and dispersion in different brain regions (Iida *et al* 1986, 1988). However, compared to brain imaging which is limited to a single organ structure, the multitude of organ structures and regions with diverse kinetics encountered in the torso region, makes kinetic modelling in the body challenging and its application within a 4D framework particularly complex. Regions with differential delay and dispersion (thoracic versus abdominal organs as well as veins carrying the activity from the injection site) and activity delivery through routes other than arterial blood (such as urinary excretion, bile, as well as venous delivery in the liver), can be located within the FOV. In such cases, a common model cannot describe the kinetics within the FOV. Therefore, due to the interleaving between tomographic and kinetic modelling steps, the erroneous kinetic model fitting in certain regions will result in the propagation of errors in the vicinity of these regions. This leads to biased kinetic parameters even in regions where the data are accurately modelled. One simple approach to minimize errors is using pre-defined masks to specify the regions where kinetic modelling can be applied, while using general models (polynomials, B-splines, … etc) in the remaining regions (Germino *et al* 2015a). However, such masks need to be defined *a priori* and require manual intervention. A more user independent approach that can alleviate the problem is the application of adaptive kinetic models. Such models rely on looking at the residuals and attempting to detect any structure which usually arises from inappropriate model fitting. When structured residuals are identified, either a different primary model (Germino *et al* 2015b) or alternatively a secondary residual model (Matthews *et al* 2012) can be used, to allow a less constrained fit. Residual models can minimize error propagation in well modelled regions when used within 4D reconstruction, yet they are difficult to implement, have free parameters to optimize and often reduce bias at the expense of increased variance due to the complexity of separating structured residuals from noise (Kotasidis *et al* 2014).

Secondly involuntary and voluntary inter/intra-frame bulk body motion (apart from cardiac and respiratory) can frequently occur in dynamic body studies (axial slide, shoulder twist, side roll, … etc) (Mukherjee *et al* 2010, Konik *et al* 2014) especially due to the longer acquisition times (>1 h) compared to static imaging (Klein *et al* 2011). Even in cases when immobilization devices are used, significant motion can occur (Green *et al* 1994, Beyer *et al* 2005). The situation is more severe in elderly patients and in those presenting with neurological/psychological disorders (e.g. Tourette syndrome, epilepsy, Parkinson) where the use of rigid restraining devices often is not tolerated. Such motion can occur either between frames or within frames and can cause significant changes in voxel-wise time-activity curves (TACs), especially on the boundaries of regions with significantly different kinetics and high activity gradient. Such blurring across frames could subsequently lead to blurring of the kinetic parameter maps (Herzog *et al* 2005, Dinelle *et al* 2011, Keller *et al* 2012) or even affect the extraction of image-derived input functions from the dynamic emission data (Mourik *et al* 2011). Furthermore, patient movement will most likely cause an emission/attenuation mismatch in the affected frames, resulting in errors during attenuation correction and scatter estimation (Anton-Rodriguez *et al* 2010, Häggström *et al* 2014). However, such emission/attenuation mismatch could also occur in the absence of any inter/intra-frame motion as patient motion could occur in the time interval between the transmission and emission acquisitions while the patient remains still during the emission scan. A number of strategies have been devised for motion correction (Jin *et al* 2013). These include online optical motion tracking systems and incorporation of motion information in image reconstruction (Bloomfield *et al* 2003, Qiao *et al*

2006, Rahmim *et al* 2007, 2008, Dinelle *et al* 2011, Olesen *et al* 2012), post-reconstruction frame-by-frame realignment methods using either optical systems or image-based algorithms (Wardak *et al* 2010, Costes *et al* 2009, Mourik *et al* 2009, Ye *et al* 2014, Jiao *et al* 2015), as well as more advanced methods leading to simultaneous estimation of motion and kinetic parameters (Jiao *et al* 2014). However, realignment methods can be tracer/activity dependent and susceptible to noise (especially in early frames) when image-based methods are used for frame-by-frame transformations. They also suffer from problems related to rigid marker fixation when optical methods are used. On the other hand, reconstruction-based approaches can be more computationally intensive and slow to converge, have difficulties to handle out-of-FOV events and are limited by the optical tracking accuracy. Therefore, in cases where no motion correction is used or residual errors remain due to the shortcomings of the selected motion correction scheme, the bias introduced either due to emission/attenuation mismatch, intra- and inter-frame motion blurring, or both, could lead to kinetic parameter error propagation (temporal or spatial) during direct 4D image reconstruction. Emission errors in certain frames and regions caused by attenuation mismatch or motion, could possibly propagate to other frames during the kinetic modelling step (temporal propagation). Subsequently, the errors in those frames could further propagate spatially during the tomographic step (spatial propagation).

Despite the fact that erroneous kinetic modelling, emission/attenuation mismatch and bulk motion are different sources of errors, all could potentially result in biased parametric maps if direct 4D methods are used, with parameter bias not only restricted to erroneous regions but further away from them. Therefore, methods to restrict the spatial propagation of errors in the dynamic emission data, which translate in error propagation in the kinetic parameter space, are needed.

Time-of-flight (TOF) imaging has been regaining considerable momentum during the last few years owing to continuous hardware and software advancements (Moses 2003, Conti *et al* 2005, Surti *et al* 2006, Conti 2009, 2011a, Surti 2015). TOF image reconstruction results in signal-to-noise ratio (SNR) improvements and apparent increase in the effective sensitivity (Budinger 1983, Conti *et al* 2013, Westerwoudt *et al* 2014). However, one benefit of TOF when used within 3D image reconstruction is the robustness it provides under the presence of inconsistent correction data, such as attenuation, scatter and normalization, as demonstrated by (Conti 2011b). Data from a point source in image space will only contribute to a specific number of TOF bins according to the TOF probability distribution. Therefore, any errors located in a certain region are more likely to be constrained in the vicinity of that region, depending on the TOF timing resolution. In an analogous way, in this work, we extrapolate this concept from errors encountered in static imaging which can propagate in 3D reconstruction, to errors appearing in dynamic imaging which propagate or could potentially propagate in direct 4D image reconstruction. We envisage that TOF-based direct 4D image reconstruction could potentially be more robust in the presence of errors arising in dynamic imaging, such as application of erroneous kinetic model fitting and inter-frame bulk body motion. The incentive behind such hypothesis is similar to the 3D case. It is based on the fact that the spatial constraints imposed by TOF information could restrict the propagation of kinetic model-induced or motion-induced errors between the tomographic steps within the 4D reconstruction and improve upon kinetic parameters in regions consistent with the TOF information.

As such, incorporating TOF information within an existing direct 4D EM framework, we develop a direct 4D TOF image reconstruction algorithm and apply it to simulated 4D dynamic $[^{15}O]H_2O$ TOF datasets to investigate kinetic model induced error propagation. Kinetic parameters are estimated using direct 4D TOF image reconstruction at different TOF resolutions as well as conventional non-TOF direct 4D reconstruction and 3D post-reconstruction kinetic analysis. Furthermore, we investigate the effect of bulk body motion on kinetic parameter

Table 1. Simulated kinetic parameters used for the [^{15}O]H_2O 1 tissue model.

	K_1 (ml/s/ml)	k_2 (ml/s/ml)	bv (ml/ml)	Vd (ml/ml)
Lungs	0.0008	0.0014	0.06	0.6
Bone	0.0018	0.0027	0.00	0.69
Soft tissue	0.0005	0.0042	0.00	0.12
Ventricles	0.0000	0.0000	1.00	0.00
Myocardium	0.0167	0.0183	0.15	0.91
Tumors	0.0098	0.0161	0.08	0.61
Liver	0.0117	0.0119	0.05	0.98

estimation and its implication in parameter estimation when direct 4D image reconstruction is used. The effects of inter-frame blurring and emission/attenuation mismatch are demonstrated separately and together.

2. Methods

2.1. Simulated dynamic datasets

To investigate the impact of inconsistencies during dynamic imaging, on the kinetic parameters, when these are directly estimated from the measured dynamic data, fully 4D dynamic datasets were simulated based on [^{15}O]H_2O kinetics. TACs represent a 3 parameter 1-tissue model (K_1, k_2), including a blood volume component (bv). A 4D digital body phantom was used, comprising of 8 major internal body structures. The anatomical information covering the thoracic and upper abdominal area were generated using MRI-derived data to segment the different regions (soft tissue, bones, liver and lungs). The myocardium and heart ventricles were segmented using an ECG triggered MRI scan, while 9 tumours of different sizes where manually inserted in the liver and lung regions (Tsoumpas *et al* 2011, Buerger *et al* 2012). In each region, kinetic parameters from a typical [^{15}O]H_2O scan were assigned (table 1). The dynamic datasets simulated a typical 6 min scan with 28 time frames (14×5 s, 5×10 s, 3×20 s, 6×30 s), and realistic as well as diverse kinetics. Based on the segmented organs that were used to generate the anatomical phantom, an attenuation map was also generated using a 4 region classification of the phantom (air: 0 cm^{-1}, lung: 0.03 cm^{-1}, soft tissue: 0.099 cm^{-1}, and bone: 0.15 cm^{-1}).

2.1.1. Inconsistent dynamic data from diverse kinetics. To investigate the impact of TOF on directly estimated kinetic parameters in the presence of diverse kinetics in the FOV, different physiological responses were assigned to the different organ regions, simulating possible discrepancies between the underlying kinetics and the common kinetic model used during parameter estimation (table 2).

All organ regions with the exception of the liver and the heart ventricles, shared a common input function (IF) using a single input model. As such, the counts within image voxels in these regions were proportional to:

$$fC_A(t) \otimes e^{-(k_2+\lambda)\cdot t} + bv \cdot C_A(t) \quad (1)$$

$C_A(t)$ is the arterial input function activity concentration over time, f is perfusion ($f = K_1$ for freely diffusable tracers, such as [^{15}O]H_2O, where permeability surface area product is high and the extraction is 100% under normal physiological conditions), k_2 is the efflux rate, bv is the fractional blood volume and λ is the decay constant of [$^{15-}$O] ($\lambda = 0.00567\,s^{-1}$).

Table 2. Input function supply and delay parameters used for the kinetic model during generation of the dynamic dataset and parameter estimation within the employed digital phantom. Inconsistencies between the model and the data are marked in bold.

	Simulated kinetics		Kinetic modeling		
Organs	Input	Delay	Input	Delay	Match
Liver	**Dual**	**No**	**Single**	No	No
Myocardium	Single	No	Single	No	Yes
Liver tumors	Single	No	Single	No	Yes
Lungs	Single	No	Single	No	Yes
Lung tumors	Single	No	Single	No	Yes
Soft tissue	Single	No	Single	No	Yes
Bones	Single	No	Single	No	Yes
Heart ventricles	**Single**	**Yes**	**Single**	No	No

To introduce diverse kinetics in the FOV, an input function with a differential delay and dispersion and representing earlier tracer arrival time, was used to generate the TAC in the heart ventricles (delay $= -8$ s, dispersion coefficient $= 0.09$) compared to the IF used to generate the TACs in the remaining regions (considering the tracer's arrival time in other regions as the reference zero time point). Furthermore, a dual input model was used in the liver (hepatic artery + portal vein) (Kudomi *et al* 2008) compared to other regions (single input model). To simulate the portal vein, the gastrointestinal compartment was introduced in the simulation, which is a single compartment model between arterial blood and the gut compartment (figure 1). No delay between the arterial and portal input function was assumed. As such, the counts within image voxels in the liver were proportional to:

$$(f_a C_A(t) + f_p C_P(t)) \otimes e^{-(k_2+\lambda)\cdot t} + bv \cdot C_a(t) \tag{2}$$

with

$$C_p(t) = k_g C_A(t) \otimes e^{-k_g \cdot t} \tag{3}$$

being the gut compartment with diffusion rate $k_g = 0.5\,\text{min}^{-1}$ and

$$k_2 = \frac{(f_a + f_p)}{\text{Vd}}, C_a(t) = r_a C_A(t) + r_p C_P(t) \tag{4}$$

$$r_a = \frac{f_a}{(f_a + f_p)}, r_p = \frac{f_p}{(f_a + f_p)} \tag{5}$$

where Vd is the volume of distribution, f_a and f_p are the arterial and portal vein blood flows while r_a and r_p are the arterial and portal vein blood flow to total hepatic flow ratios, respectively.

2.1.2. Inconsistent dynamic data from emission–transmission mismatch. To investigate the impact of TOF on directly, as well as indirectly estimated kinetic parameters in the presence of emission–transmission mismatch, a relative shift was introduced between the simulated dynamic emission data and the corresponding attenuation map. Thus the dataset simulated the situation of the patient moving between the emission and transmission scans, but remaining motion free for the duration of the emission scan. All 28 time frames were rotated and translated (Vinci software, Max-Planck-Institute) based on realistic situations, representing rigid bulk body motion (translations: ($x = 2$ mm, $y = 3.5$ mm, $z = 6.5$ mm), rotations: ($\vartheta x = 1.3°$,

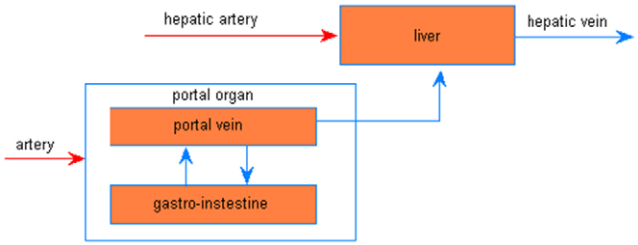

Figure 1. Schematic diagram showing the dual input model with both the hepatic artery and portal vein supplying blood to the liver. The venous blood in the portal vein is drained from the gastro-intestine organs with the blue arrows representing equilibration between tissue and venous concentrations.

$\vartheta y = 2°$, $\vartheta z = 1.3°$]. Figure 2 shows the attenuation maps at the original position as well as the attenuation mismatch between the 2 positions (before and after patient movement).

2.1.3. Inconsistent dynamic data from inter-frame motion. To investigate the impact of TOF on estimated kinetic parameters in the presence of inter-frame motion, an inter-frame patient movement was simulated between the 11th and 21st frames. The simulated rigid bulk body motion (translations: ($x = 2$ mm, $y = 3.5$ mm, $z = 6.5$ mm), rotations: ($\vartheta x = 1.3°$, $\vartheta y = 2°$, $\vartheta z = 1.3°$) corresponded to the patient moving to a new position at the 11th frame and returning back in the original position after the 21st frame. No intra-frame motion was simulated. The effect of inter-frame blurring and emission/attenuation mismatch were evaluated separately and together. First, the motion affected data were reconstructed using the correct attenuation maps corresponding to each frame and simulating only the emission blurring between frames. Secondly, the emission/attenuation mismatch was also considered as well, therefore using a common attenuation map for all temporal frames, corresponding to the original position. The 3 simulated scenarios regarding inter-frame motion and emission/attenuation mismatch are depicted in figure 3.

2.2. Projection data

A virtual TOF PET scanner corresponding to the geometry configuration of the mCT PET/CT scanner (Siemens Healthcare, Erlangen), was used to generate the dynamic TOF datasets (span 11, 7 segments, maximum ring difference of 38, angular mash factor of 2) based on an in-house TOF projection simulator. Dynamic TOF projection data were generated at 4 different TOF resolutions using a TOF kernel with 580 ps (13 TOF bins), 440 ps (17 TOF bins), 300 ps (27 TOF bins) and 160 ps (49 TOF bins) full width at half maximum (FWHM), as well as non-TOF data (radial_bins (400) $\times$ angles (200) $\times$ sinogram planes (303) $\times$ dynamic frames (28) $\times$ TOF bins (1, 13, 17, 27 or 49)). To isolate the impact of TOF on bias propagation, only noiseless datasets were considered, as TOF influences the SNR and as such, it would be difficult to decompose any bias due to error propagation from the noise induced bias.

2.3. Image reconstruction and kinetic modelling

Kinetic parameter estimation from the simulated dynamic datasets was performed using both traditional 3D image reconstruction followed by kinetic modelling, as well as direct 4D image reconstruction, without as well as with TOF at different TOF resolutions (580 ps,

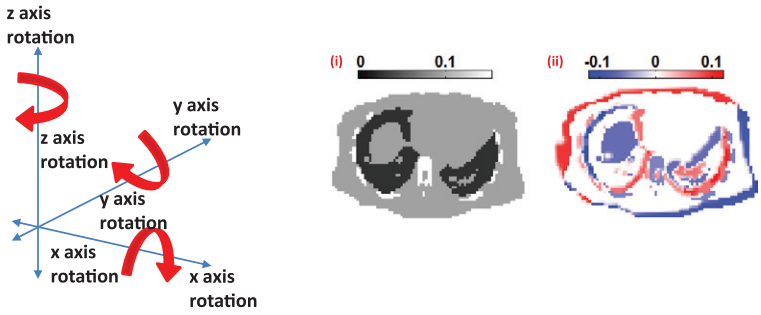

Figure 2. The emission/attenuation mismatch was simulated by introducing rotations and translations on the emission data. The attenuation map is shown along with the bias introduced in the attenuation map used during image reconstruction due to motion-induced emission–transmission mismatch.

440 ps, 300 ps, and 160 ps). The direct 4D TOF reconstruction was based on our conventional EM-based direct 4D framework, which allows separation between the tomographic and kinetic modelling steps. This algorithm, is based on converting the spatiotemporal 4D maximum likelihood problem in projection space,

$$\boldsymbol{\alpha}^{\text{opt}} = \arg\max_{\alpha} \sum_{il} (m_{il} \log_e(y_{il}) - y_{il}) \tag{6}$$

$$y_{il} = \sum_j p_{ij} \lambda_{jl} + \eta_{il} = \sum_j p_{ij} f_{jl}(\boldsymbol{\alpha}) + \eta_{il} \tag{7}$$

where during the lth time frame and in the ith data bin, m_{il} are the PET measured data, y_{il} the mean number of events, η_{il} the mean number of erroneous events, p_{ij} the probability system matrix of a photon emitted from the jth voxel and being detected in the ith projection bin and λ_{jl} is the number of emissions from the jth voxel in the image during the lth time frame described by a kinetic model f_{jl} with parameter vector $\boldsymbol{\alpha}$; into a maximum likelihood problem in image space

$$\boldsymbol{\alpha}^{(k+1)} = \arg\max_{\alpha} \sum_j (\sum_i p_{ij}) \sum_l (\lambda_{jl}^{(k+1)} \log_e(f_{jl}(\boldsymbol{\alpha})) - f_{jl}(\boldsymbol{\alpha})) \tag{8}$$

where

$$\lambda_{jl}^{(k+1)} = \frac{f_{jl}(\boldsymbol{\alpha}^{(k)})}{\sum_i p_{ij}} \sum_i \frac{p_{ij} y_{il}}{\sum_{j'} p_{ij'} f_{j'l}(\boldsymbol{\alpha}^{(k)}) + \eta_{il}} \tag{9}$$

Using a one step late approach, equation (8) can be approximated with a weighted least square problem

$$\boldsymbol{\alpha}^{(k+1)} = \arg\min_{\alpha} \frac{1}{2} \sum_{jl} w_{jl}(\boldsymbol{\alpha}) (\lambda_{jl}^{(k+1)} - f_{jl}(\boldsymbol{\alpha}))^2 \tag{10}$$

where the weights are given by

$$w_{jl}(\boldsymbol{\alpha}) = \frac{1}{f_{jl}(\boldsymbol{\alpha})} \tag{11}$$

with k being the number of iterations.

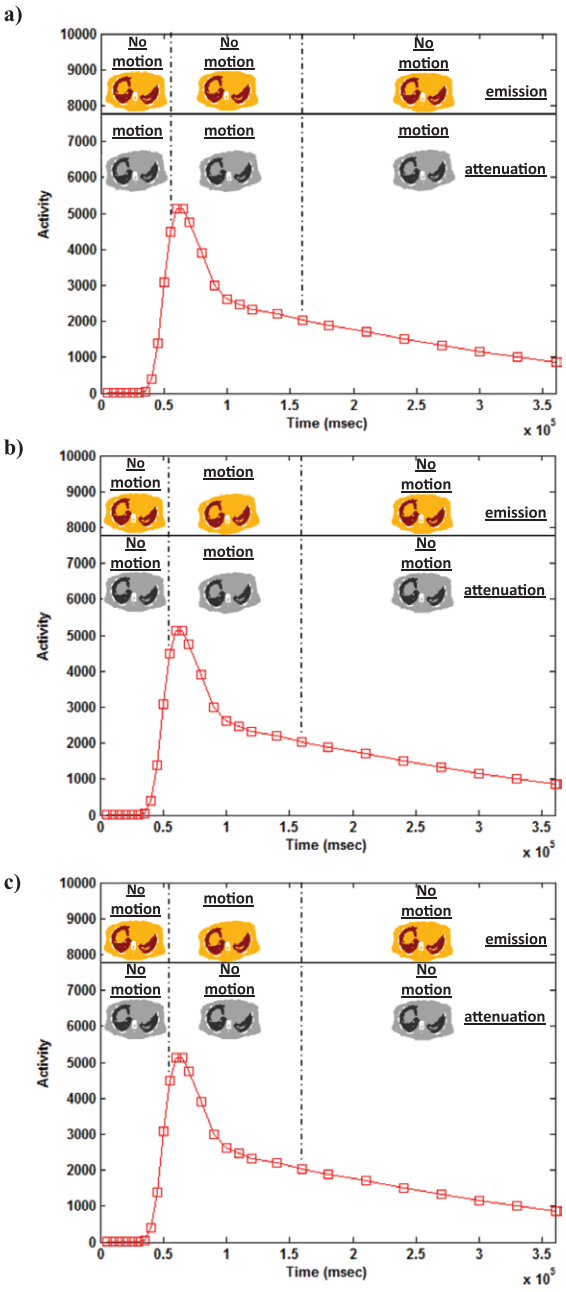

Figure 3. Three individual cases were simulated to investigate the effects of bulk body motion. First, the case of a mismatch between the emission and attenuation maps due to patient movement after the transmission scan but without motion during the emission scan (a). Second, the case of a patient moving between frames 11–21 (55–160 s) but using the correct attenuation map for each frame, therefore isolating the effect of inter-frame blurring only (b). Third, having the same situation as in the second case but including also the emission/attenuation mismatch by using a single attenuation map for the entire dynamic scan, therefore not only having an inter-frame blurring in frames 11–21 but also a mismatched attenuation (c).

The algorithm proceeds by alternating between the tomographic EM image update (equation (9)) and the voxelwise image-based least squares kinetic modelling steps (equation (10)).

Extending this algorithm to direct 4D TOF image reconstruction was done by incorporating TOF projectors into the tomographic step. TOF projectors were implemented using pre-computed non-symmetric TOF weighting coefficients taking into account the geometric symmetries in the scanner during their application. Therefore the TOF equivalent of equation (9) can be expressed as:

$$\lambda_{jl}^{(k+1)} = \frac{f_{jl}(\boldsymbol{\alpha}^{(k)})}{\sum_i \sum_t z_{ijt}} \sum_i \sum_t \frac{z_{ijt} y_{itl}}{\sum_{j'} \sum_t z_{ijt} f_{j'l}(\boldsymbol{\alpha}^{(k)}) + \eta_{itl}} \tag{12}$$

where y_{itl} is the expected number of events in the ith projection bin, tth time bin and lth temporal frame ($y_{il} = \sum_t y_{itl}$), z_{ijt} is the probability of an event emitted from the jth voxel being detected in tth time bin along the ith LOR and η_{itl} is the mean number of erroneous events in the ith projection bin, tth time bin and lth temporal frame including randoms and scattered contributions. Random events are TOF independent and equally distributed amongst time bins, while scattered events have a TOF dependence. The elements of the TOF weighting coefficient matrix are calculated using a Gaussian modelled TOF kernel, with the probability of an event detected at the tth TOF bin, given a time difference δ, calculated as the definite integral of the TOF kernel between the time boundaries of the tth TOF bin and centred at δ time point (Mehranian *et al* 2016). TOF 3D reconstruction resembles the tomographic part of the direct 4D TOF reconstruction (equation (12)) with the difference being that the previous image estimate is not the fitted image following kinetic modelling and described by a kinetic model f_{jl} with parameter vector $\boldsymbol{\alpha}$, but the previous tomographic image estimate.

$$\lambda_{jl}^{(k+1)} = \frac{\lambda_{jl}^{(k)}}{\sum_i \sum_t z_{ijt}} \sum_i \sum_t \frac{z_{ijt} y_{itl}}{\sum_{j'} \sum_t z_{ij't} \lambda_{j'l}^{(k)} + \eta_{itl}} \tag{13}$$

Both 3D and 4D image reconstructions were OSEM-based (21-subsets and up to 16 iterations), while no scatter and randoms contributions were taken into account.

For the kinetic model, we used a 3 parameter, 1-tissue single arterial input model including a blood volume term, with no delay and dispersion in the IF. The generalized linear least square (GLLS) method was used to generate parametric maps while the linear least square (LLS) method was used to initialize the kinetic parameters for GLLS (2 iterations) (Feng *et al* 1996).

3. Results

3.1. Inconsistent dynamic data from diverse kinetics

In regions where the data are inconsistent with the model, such as the heart ventricles and liver, TACs appear biased (figure 4) when kinetic analysis is performed following traditional 3D reconstruction. In the remaining regions, where the dynamic data are consistent with the kinetic model, TACs appear to have almost converged to the real simulated TACs. When direct 4D reconstruction is used, the TACs in those regions appear biased due to the additional errors propagated between the tomographic and kinetic modelling steps. This is apparent when looking at the TAC from the myocardium (figure 4(A)).

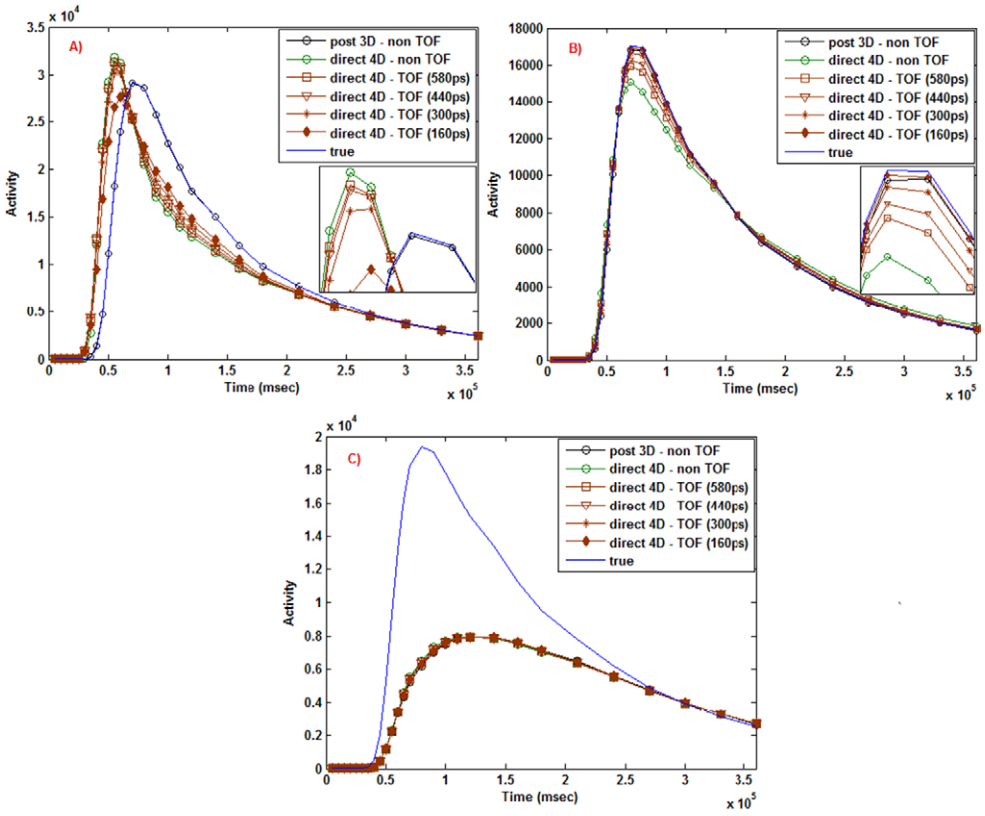

Figure 4. Time-activity curves (TACs) from the entire myocardium (A) and lungs (B) regions, representing regions for which the dynamic data are consistent with the model used for parameter estimation and from the liver (C), representing a region for which the data are inconsistent with the kinetic model. TACs are plotted using post-reconstruction kinetic analysis, direct 4D reconstruction and direct 4D TOF reconstruction at improving TOF resolutions (FWHM). The true simulated TACs are also shown for comparison. Both the myocardium and lung TACs are affected by error propagation in direct 4D reconstruction, with the inclusion of TOF gradually reducing propagation and matching the reconstructed to the simulated TACs as well as those following post-reconstruction analysis. In the liver, being an erroneously modelled region, all methods match since TOF appears not to improve upon the actual error but only its propagation.

The activity in the heart ventricles arrives earlier and less dispersed compared to the rest of the regions, therefore causing the activity in the myocardium to arrive earlier and be less dispersed as well. Similar propagation of errors is seen in the lung TAC which is mostly affected by the liver bias. When TOF information is used within 4D reconstruction, the TACs in these well modelled regions appear to get closer to the simulated TACs and similar to the post-reconstruction analysis. In the lungs, the improvements are correlated with the ever improving TOF resolution. However, improvements in the myocardium, are only noticeable at 160 ps as the myocardium is relatively small and surrounded by the erroneously modelled ventricles. Therefore, high TOF resolutions are needed to start decoupling the influence of voxels from the ventricles into the myocardium. In the regions, where the data are inconsistent with the model, all reconstruction methods are matched since TOF doesn't appear to impact upon the errors, but only on their propagation.

Parametric images of K_1, Vd and blood volume were estimated using both traditional post-reconstruction kinetic analysis and direct 4D reconstruction and are shown along with the corresponding bias maps in figure 5. When maps are estimated with post-reconstruction analysis, the erroneous kinetic model in the liver and heart ventricles introduced parameter bias in these regions of up to 90%. However, the errors are restricted to these 2 regions, which is in contrast with what is observed when the parameters are directly estimated from 4D reconstruction (also seen from the TACs). Errors spatially propagate to other regions for which the model is consistent with the measured data and regional errors in the lungs, myocardium and soft tissue of up to 50% can be seen. The severity of this bias appears to be spatially dependent and more pronounced closer to the regions where the data are not consistent with the kinetic model. By using TOF information within 4D reconstruction, errors appears to be reduced even at 580 ps, while at 160 ps the observed bias propagation is restricted close to the boundaries of the erroneously modelled regions. This is more pronounced when looking at the soft tissue in the boundaries of the heart ventricles, while the myocardium is still biased even at 160 ps due to its vicinity to the ventricles (being erroneously modelled). These improvements demonstrated at improving TOF resolutions, persevere at higher number of iterations despite the fact that all the parameter estimation methods have different convergence rates. This can be seen in figure 6 where the overall bias in the phantom for K_1, Vd and blood volume is plotted for all parameter estimation methods and for increasing number of image updates (8 iter, 21 subsets). As expected, TOF-based 4D reconstructions converge faster, with the rate increasing at higher TOF resolutions. Furthermore, the observed bias reduction appears to be non-linearly related to the TOF resolution improvements. The bias reduction in all parameters going from 300 ps to 160 ps appears consistently higher (K_1 ~ 3%, Vd ~ 5%, bv ~ 5%) than going from 580 ps to 440 ps (K_1 ~ 1%, Vd ~ 2%, bv ~ 2%), despite TOF resolution improving by 140 ps in both cases, respectively. In addition, it can also be seen that despite an almost 10% bias reduction between non-TOF and TOF (160 ps) 4D reconstructions, the residual bias still persists compared to the post-reconstruction analysis. Nevertheless, additional K_1 and Vd parameter bias from propagation is reduced to less than 4% compared to ~15% and 25%, respectively, when TOF is not used.

3.2. Inconsistent dynamic data from emission–transmission mismatch

Inconsistencies between the kinetic model and the dynamic data can cause errors that propagate in 4D reconstruction as shown previously. However, other inconsistencies such as inter-frame motion could potentially cause similar error propagation. To investigate first the effect of emission/attenuation mismatch separately from inter-frame emission blurring, patient movement was simulated between the transmission and dynamic emission scan but without any motion during the emission scan. In figure 7(A), TACs are plotted for post-reconstruction analysis and direct 4D reconstruction without and with TOF at ever improving TOF resolutions. Both 3D as well as direct 4D reconstructed TACs appear to be negatively biased by up to 35% across all frames. However, incorporating TOF, a gradual decrease in bias can be seen going towards improved TOF resolutions. The bias is reduced to ~17% at 580 ps, with further reduction to less than 7% at 160 ps. Comparing the 3D against the direct 4D reconstruction, a difference of up to 4% was seen when TOF is not used (especially in the late frames), with the 2 methods giving almost identical TACs at the highest TOF resolution (160 ps). Parametric maps are shown in figure 8 for both 3D and direct 4D methods, whereas the corresponding bias maps are displayed in figure 9. Similar to what has been observed on the TAC plots (figure 7), all parameters appear significantly biased in both parameter estimation methods and in the absence of TOF information. The bias appears to be higher in the boundaries of regions with

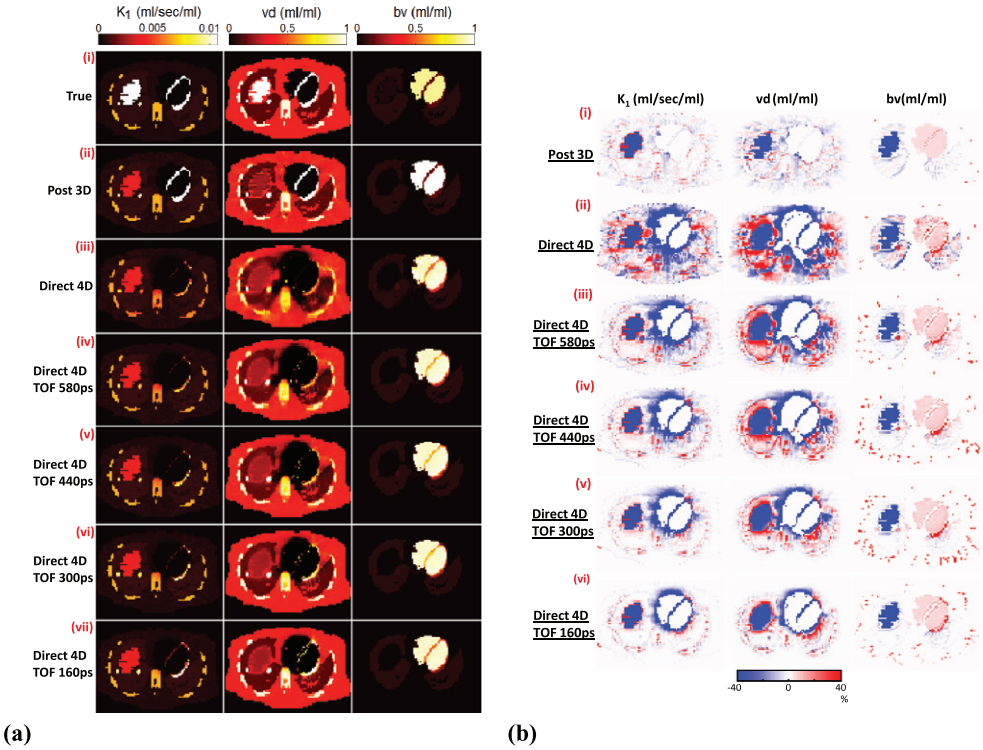

Figure 5. True (a-i) and estimated kinetics parameter maps using post-reconstruction (a-ii), non-TOF direct 4D (a-iii) and TOF direct 4D ((a-iv)–(a-vii)), parameter estimation methods. Using post-reconstruction kinetic analysis, the inconsistencies introduced in the liver and heart ventricles result in bias in those 2 regions. Using direct 4D reconstruction, these errors spatially propagate as expected to other regions. By incorporating TOF information, a gradual bias reduction is observed with errors almost suppressed in the immediate vicinity of those 2 erroneously modelled regions (liver and ventricles), resembling the post-reconstruction approach. The corresponding bias parametric maps are shown for the post-reconstruction (b-i), non-TOF direct 4D (b-ii) and TOF direct 4D ((b-iii)–(b-vi)), parameter estimation methods.

high attenuation gradient; however, the bias is present in other regions as well. Inclusion of TOF information appears to gradually reduce the bias caused by attenuation errors throughout the body. Using direct 4D reconstruction, similar improvements can be seen at improving TOF resolutions. However, quantitative analysis on the bias maps between post reconstruction analysis and direct 4D reconstruction revealed additional parameter bias when parameters are directly estimated. In figure 10, parameter bias in the lungs is plotted as a function of image updates for all parameter estimation methods. In the absence of TOF, parameters estimated directly are consistently more biased (K_1 ~ 60%, Vd ~ 40%, bv ~ 36%) compared to conventional post-reconstruction analysis (K_1 ~ 58%, Vd ~ 37%, bv ~ 35%) across image updates. Such difference could be attributed to attenuation errors, which are already spatially propagating within 3D reconstruction, propagating further within 4D reconstruction. Including TOF and going towards better TOF resolutions, the errors due to propagation in 4D reconstruction are consistently and gradually reduced to less than 0.5% across all parameters at 160 ps. Absolute bias also appeared to be reducing from ~60% to <20% in K_1, from ~40% to ~15% in Vd and from ~35% to <15% in blood volume at 160 ps FWHM.

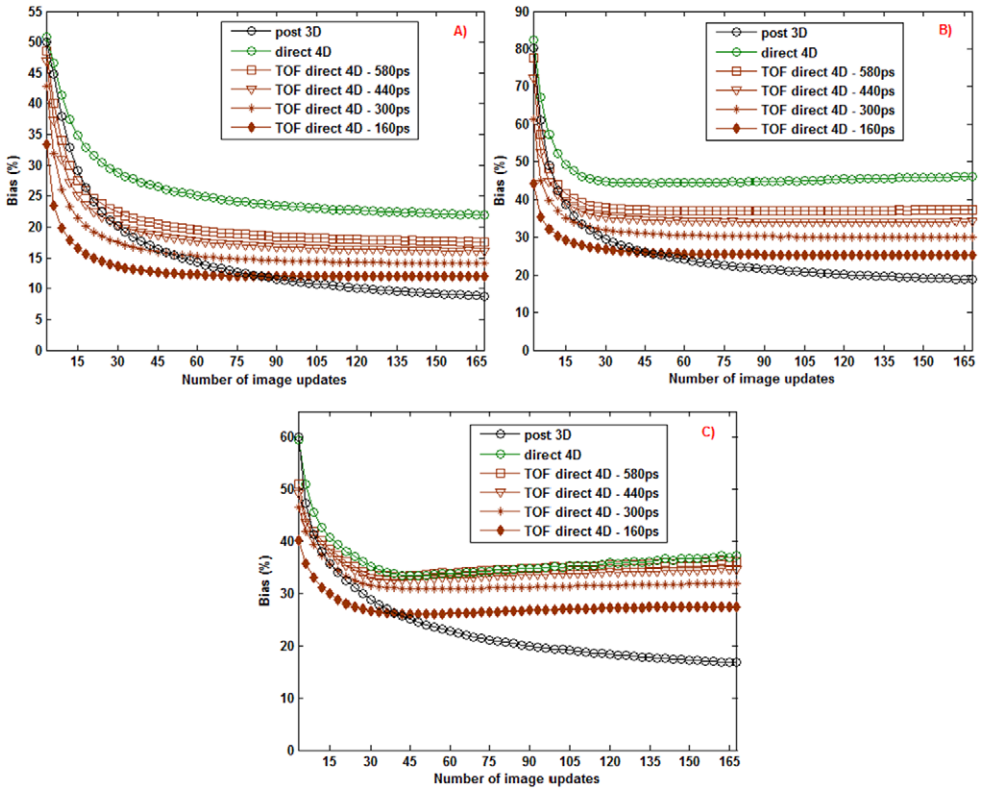

Figure 6. Graphs of K_1 (A), Vd (B) and blood volume (C) percentage bias (over all voxels) in the simulated phantom as a function of image updates (8 iterations, 21 subsets) using post-reconstruction kinetic analysis, direct 4D image reconstruction as well as TOF direct 4D image reconstruction at improving TOF resolutions (580 ps, 440 ps, 300 ps and 160 ps FWHM). Parameter bias at improving TOF resolutions is converging faster; however, bias improvements are sustained even at increased number of image updates.

3.3. Inconsistent dynamic data from inter-frame motion

To evaluate the impact of inter-frame bulk body motion on kinetic parameters, as well as the influence of TOF on them, 2 different cases were considered in order to decompose the effect of the emission blurring between frames from the emission/attenuation mismatch. The first case simulates the effect of inter-frame blurring alone, with the patient moving between frames 11–21 but using the corresponding attenuation map in each frame, while the second case considers additionally the emission/attenuation mismatch based on using a single attenuation map for all time frames. TACs from the lung region are shown in figures 7(B)–(C) for both cases considered. When only inter-frame motion is simulated (figure 7(B), a sudden dip in the TACs is seen due to the blurring of activity between the lungs and the soft tissue mainly. TACs from the 3D reconstructed dynamic data appear to match irrespective of including TOF in the reconstruction, since the individually reconstructed frames have no errors as the correct attenuation maps are used. Therefore, as the only error is the relative motion between frames 11–21 and the rest of the frames, TOF has no influence on the derived TACs. However, using direct 4D reconstruction, late frames (beyond the 21st frame)appear biased, since the interleaved tomographic and kinetic modelling steps appear to affect activity in frames for which

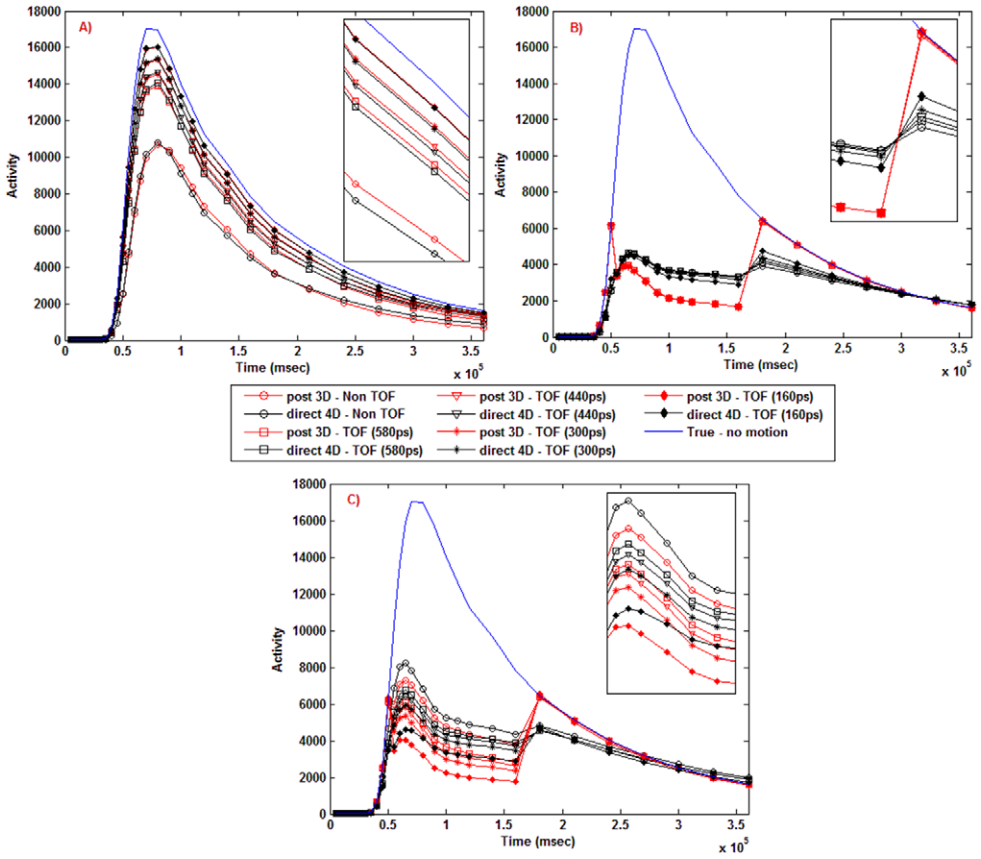

Figure 7. Time-activity curves (TACs) from the entire lung region after (A) introducing an emission/attenuation mismatch, (B) introducing an inter-frame motion between frames 11th–21st but using the correct attenuation maps in each frame and (C) finally introducing both inter-frame motion and emission/attenuation mismatch. TACs are shown for conventional post-reconstruction kinetic analysis and direct 4D reconstruction both without as well as TOF at improving TOF resolutions (580 ps, 440 ps, 300 ps and 160 ps).

no motion was simulated. Inclusion of TOF information with progressively improving TOF resolutions, gradually reduced the bias in these late frames. These findings were confirmed following kinetic modelling of the dynamic data. Figure 11 shows the estimated parametric maps for both post-reconstruction analysis and direct 4D reconstruction methods while in figure 12 the corresponding bias maps are displayed for improving TOF resolutions. Parameter bias with conventional post-reconstruction analysis is matched across all TOF resolutions and identical to non-TOF post-reconstruction analysis. Quantitative analysis for a lung ROI (figure 13) confirms that TOF has no influence since there is no temporal/spatial propagation of motion-induced inter-frame errors, while activity within each frame is correctly estimated in the absence of attenuation-induced errors. The bias converges at a different rate but almost reaches a plateau for all reconstructions (K_1 ~ 16.5%, Vd ~ 52%, bv ~ 38%) subject to using a sufficient number of iterations.

Furthermore, looking at the bias maps (figure 12), errors are localized in the boundaries of regions where TACs were blurred from inter-frame motion, due to activity gradients

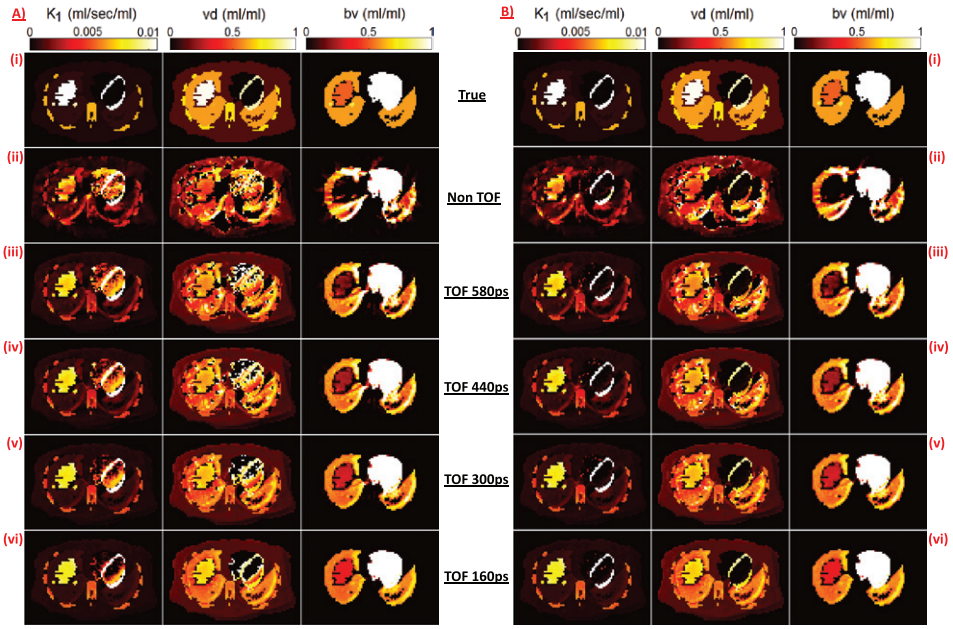

Figure 8. True (i) and estimated kinetics parameter maps without (ii) and with TOF at improving TOF resolutions (iii–vi) for both post-reconstruction kinetic analysis (A) and direct 4D image reconstruction (B) methods simulating the case of motion between emission/transmission causing an emission/attenuation mismatch.

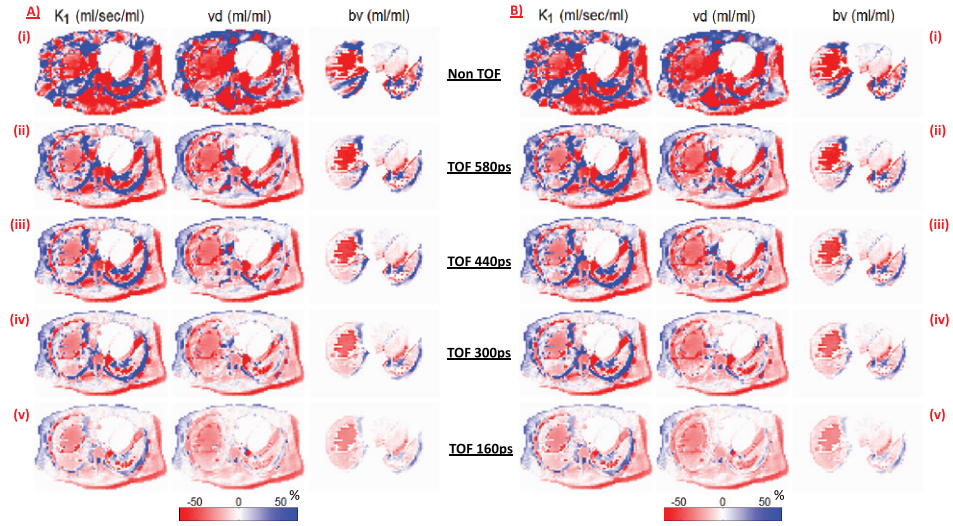

Figure 9. Bias parametric maps estimated without (i) and with TOF at improving TOF resolutions (ii–v) for both post-reconstruction kinetic analysis (A) and direct 4D image reconstruction (B) methods simulating the case of motion between emission/transmission causing an emission/attenuation mismatch.

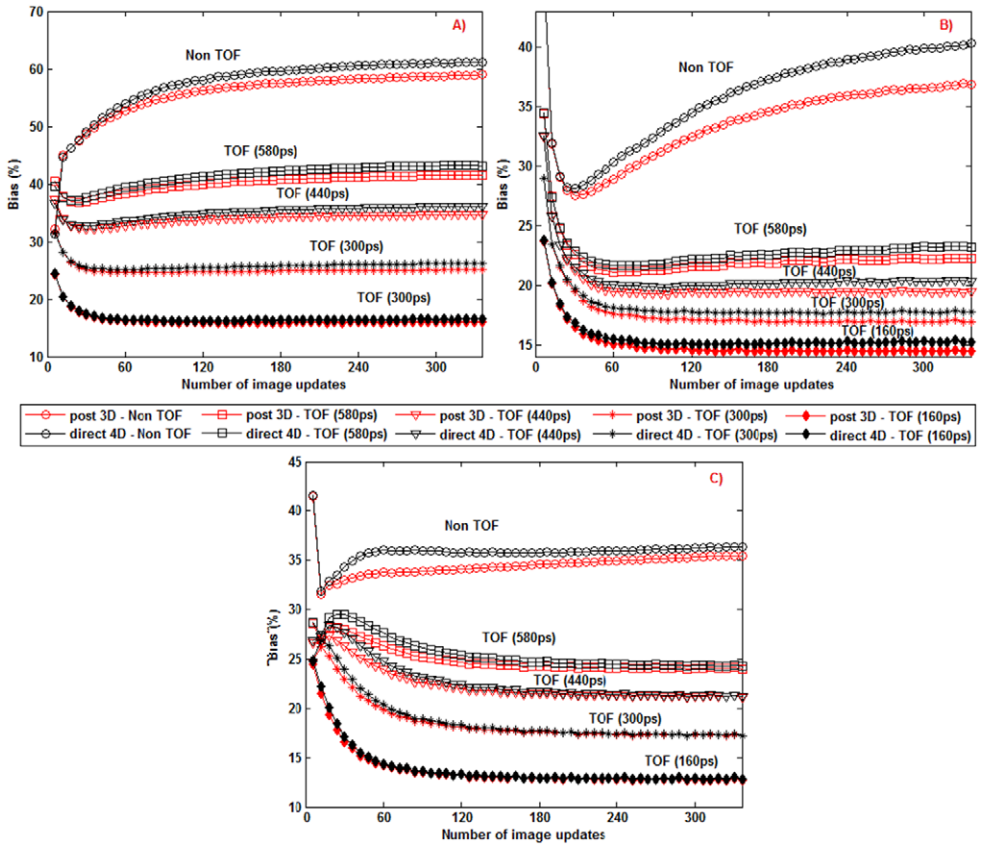

Figure 10. Graphs of (A) K_1, (B) Vd and (C) blood volume percentage bias due to motion between emission–transmission causing an emission/attenuation mismatch. The bias is shown for the lungs region as a function of image updates (16 iterations, 21 subsets) using post-reconstruction kinetic analysis and direct 4D image reconstruction without as well as with TOF at improving TOF resolutions (580 ps, 440 ps, 300 ps and 160 ps FWHM).

between regions. Positive and negative bias occurs depending on the relative activity differences between adjacent regions. However, since within each region the activity is simulated as being constant, inter-frame motion doesn't introduce blurring in the TACs further away from the boundaries and therefore kinetic parameter bias is almost zero. When parameters are estimated directly, what becomes immediately apparent is an increase in bias, which extends not only in the boundary regions but in other regions for which the TACs should be unaffected by the inter-frame motion (seen in the post-reconstruction parameter bias maps).

Errors through propagation appear to be more severe in Vd, followed by errors in K_1 and blood volume. Quantitative analysis in the lungs region (figure 13) confirms this propagation of errors, with K_1, Vd and blood volume bias in non-TOF 4D reconstruction up to ~24%, ~76% and ~42%, respectively (compared to ~16.5%, ~52% and ~38% in post-reconstruction analysis, respectively). However, in contrast to the post-reconstruction analysis, inclusion of TOF appears to improve bias, with improvements again more noticeable at improving TOF resolutions. K_1 and Vd bias in the lungs reduces by $>2\%$ with blood volume improvements being minimal ($<0.5\%$). The impact of TOF appears to be similar to the one seen in figure 6,

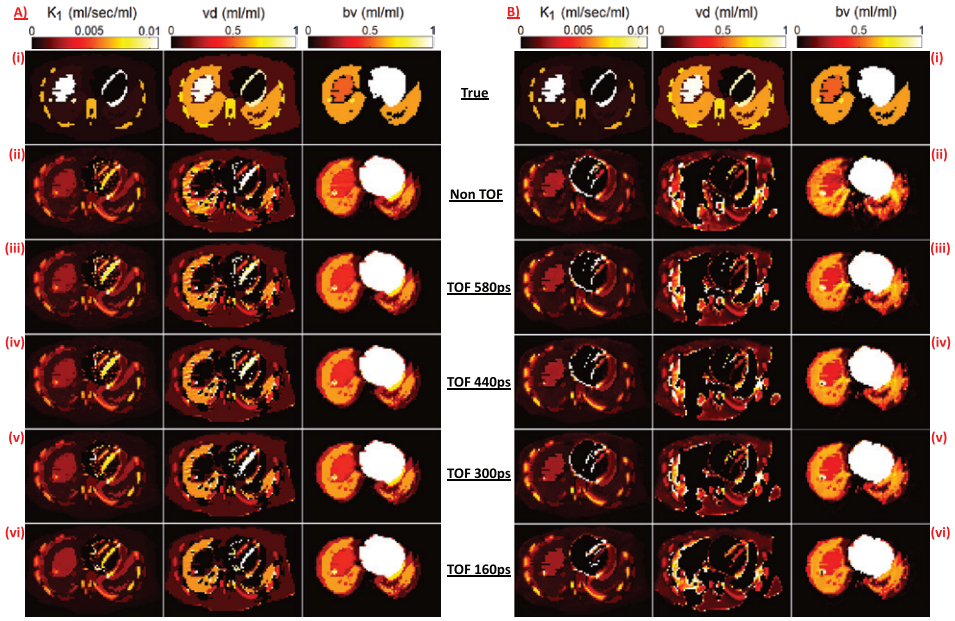

Figure 11. True (i) and estimated kinetics parameter maps without (ii) and with TOF at improving TOF resolutions (iii–vi) both for post-reconstruction kinetic analysis (A) and direct 4D image reconstruction (B) methods simulating the case of activity blurring alone due to inter-frame motion between 11th–21st frames.

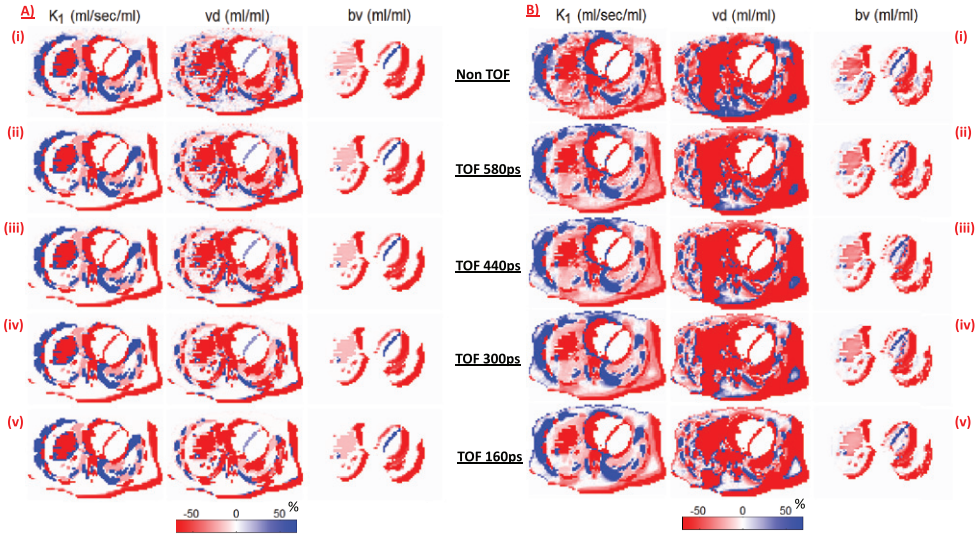

Figure 12. Bias parametric maps estimated without (i) and with TOF at improving TOF resolutions (ii–v) both for post-reconstruction kinetic analysis (A) and direct 4D image reconstruction (B) methods simulating the case of activity blurring alone due to inter-frame motion between 11th–21st frames.

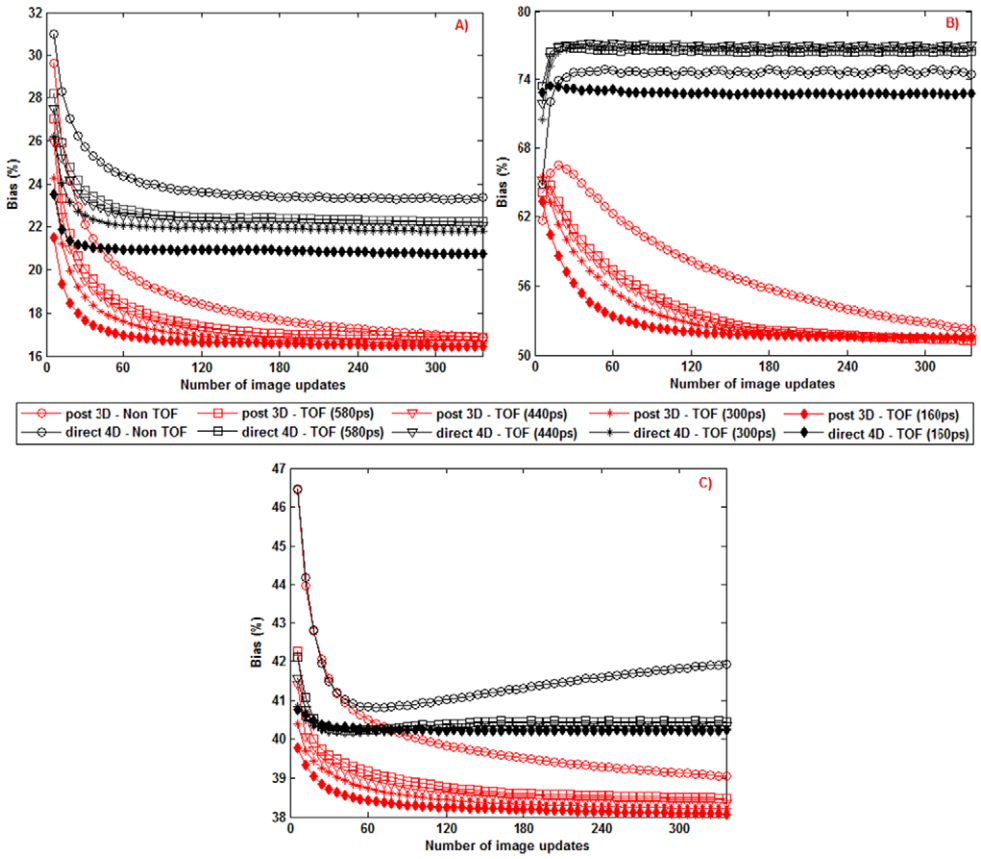

Figure 13. Graphs of K_1 (A), Vd (B) and blood volume (C) percentage bias from activity blurring due to inter-frame motion between 11th–21st frames. The bias is shown for the lungs region as a function of image updates (16 iterations, 21 subsets) using post-reconstruction kinetic analysis and direct 4D image reconstruction without and with TOF at improving TOF resolutions (580 ps, 440 ps, 300 ps and 160 ps FWHM).

with the inclusion of the TOF kernel reducing the propagation of errors in direct 4D reconstruction, though attributed to a different source of error.

It has to be emphasized that since each region in the phantom has uniform activity, inter-frame motion will result in inter-frame blurring only in the boundaries of each region/organ. Therefore regional analysis taking into account the entire organ region will result in an average error between the blurred boundaries and the rest of the organ/region for which there is no apparent change in the activity across frames (other than the normal tracer's distribution). This is the reason why TOF appears to reduce bias in the 4D reconstructed data. The errors existing in the boundaries of regions due to inter-frame motion and which propagate temporally during the kinetic modelling step in 4D reconstruction, also propagate spatially during the tomographic step. Therefore, the apparent bias reduction achieved with TOF doesn't affect the errors in the boundary of regions caused by inter-frame motion, which are unavoidable. However, it restricts their spatial propagation within each frame to a certain extent and within the limits of TOF resolution.

Introducing the effects of emission/attenuation mismatch on top of the inter-frame blurring, causes additional errors and further propagation of these errors. TACs from the lungs

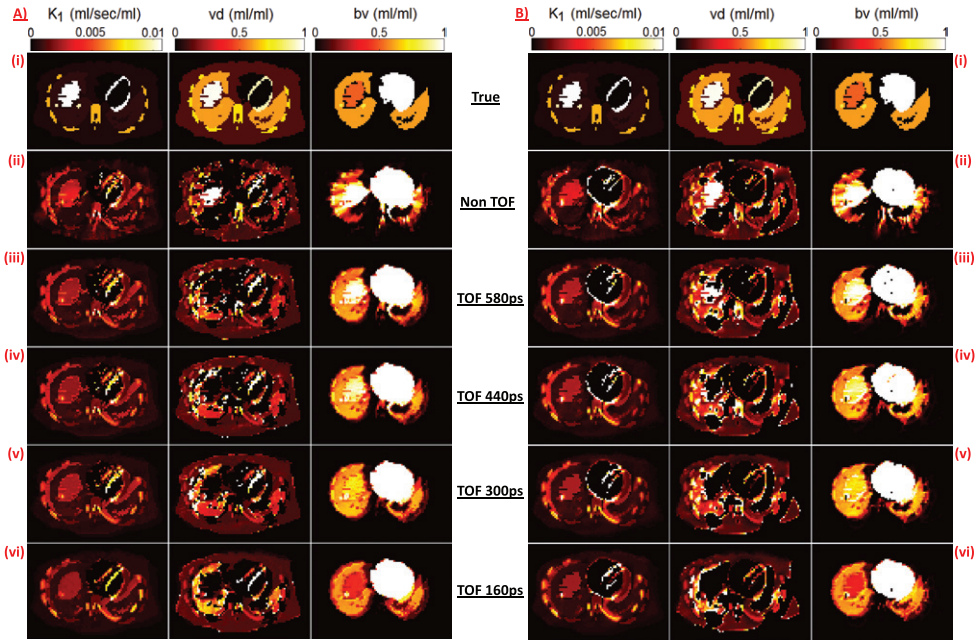

Figure 14. True (i) and estimated kinetics parameter maps without (ii) and with TOF at improving TOF resolutions (iii–vi) for both post-reconstruction kinetic analysis (A) and direct 4-D image reconstruction (B) methods simulating the case of activity blurring, as well as emission/attenuation mismatch due to inter-frame motion between 11th–21st frames.

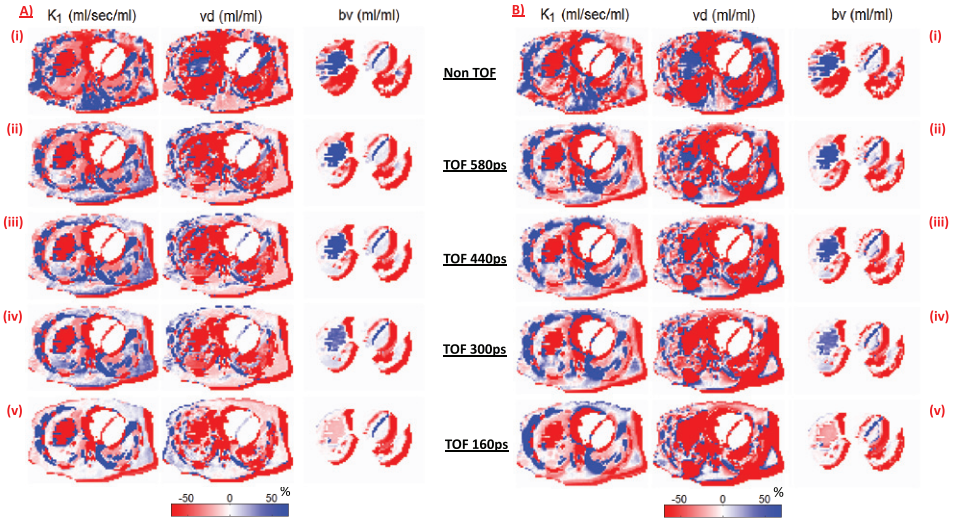

Figure 15. Bias parametric maps estimated without (i) and with TOF at improving TOF resolutions (ii-v) for both post-reconstruction kinetic analysis (A) and direct 4-D image reconstruction (B) methods simulating the case of activity blurring, as well as emission/attenuation mismatch due to inter-frame motion between 11th–21st frames.

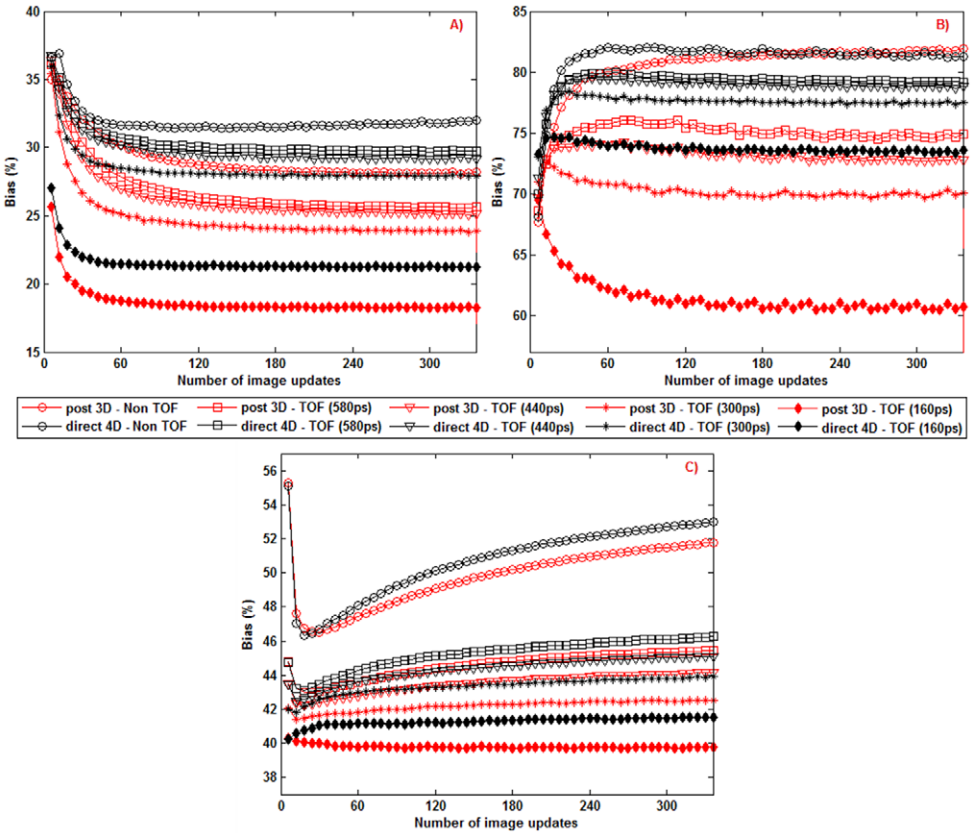

Figure 16. Graphs of K_1 (A), Vd (B) and blood volume (C) percentage bias from activity blurring, as well as emission/attenuation mismatch due to inter-frame motion between 11th–21st frames. Bias is shown for the lungs region as a function of image updates (16 iterations, 21 subsets) using post-reconstruction kinetic analysis and direct 4D image reconstruction without as well as with TOF at improving TOF resolutions (580 ps, 440 ps, 300 ps and 160 ps FWHM).

are shown again in figure 7(C) for all parameter estimation methods. In contrast to simulating the inter-frame blurring alone, when both effects are considered, inclusion of TOF within 3D reconstruction appears to change the dynamic data. The TAC at 160 ps appears similar to the 3D reconstructed TACs in figure 7(B), effectively almost negating the effect of introducing an erroneous attenuation. This can be explained by the fact that attenuation errors originate in the tomographic step and act within each individually reconstructed frame, whether in 3D or 4D reconstruction. Therefore, TOF appears to substantially suppress their impact. Dynamic data using direct 4D reconstruction again appears to be more biased compared to 3D reconstruction. However, now errors occur from 2 sources (both attenuation errors during the tomographic step of the erroneously attenuated frames which are also seen in 3D reconstructed data, and inter-frame activity blurring). These temporally propagate first in frames for which no motion or attenuation errors exist (during the kinetic modeling step), while at a second stage propagate spatially within these frames (during the tomographic step). When TOF is used within direct 4D reconstruction, TACs follow the same trend seen in the 3D reconstructed data, with the differences between 3D and 4D reconstruction at 160 ps being similar

to when no attenuation mismatch was simulated. Figure 14 shows the estimated parametric maps both for post-reconstruction analysis and direct 4D reconstruction methods while in figure 15 the corresponding bias maps are displayed for improving TOF resolutions. Looking at the bias maps, it can be seen that in post-reconstruction analysis and when TOF is not used, the bias appears not only in the boundaries of regions where attenuation mismatch occurs but also in other regions for which no attenuation mismatch occurs (considering that we simulated uniform attenuation within regions). This is similar to what was observed in figure 9 where the bias from attenuation mismatch was evaluated individually and signifies propagation of attenuation errors within each individually reconstructed frame. Quantitative analysis in figure 16 reveals that bias (in the lungs) has jumped to ~29%, ~82% and ~52% in K_1, Vd and blood volume, respectively, compared to ~16.5%, ~52% and ~38%, respectively (figure 13) when no attenuation mismatch was included. The additional bias is due to either attenuation errors in the lung boundaries, or to attenuation errors propagating in the rest of the lung (since the bias is estimated for the entire lung region). TOF, however, appears to dramatically reduce the attenuation-induced bias as seen in the bias maps (figure 15), which is also reflected in the quantitative analysis, with bias dropping by ~10% in K_1, ~7% in Vd and ~12% in blood volume at 160 ps FWHM. Looking at the directly estimated kinetic parameters, error propagation consistently persists across all not-TOF and TOF reconstructions. However, the comparison of the non-TOF direct 4D estimated parameters in figure 16 with those in figure 13 where no attenuation mismatch was included, shows that the additional effect of attenuation mismatch has increased bias in K_1, Vd and blood volume by ~8% (~24% to ~32%), ~5% (~76% to ~81%) and ~11% (~42% to ~54%), respectively. This increase in bias is less than the equivalent increase in the non-TOF post-reconstruction analysis, which stands at ~10% (~19% to ~29%) in K_1, ~30% (~52% to ~82%) in Vd and ~13% (~39% to ~52%) in blood volume. Therefore, attenuation-induced bias in the presence of inter-frame blurring appears to affect the post-reconstruction estimated parameters more than the ones directly estimated and with the error propagation from the 2 sources of errors not being simply the summation of the errors propagating from the individual effects. Inclusion of TOF also reduces errors in directly estimated parameters mostly due to the effect of TOF on attenuation and less to inter-frame blurring, as the magnitude of improvements going from non-TOF to TOF at 160 ps is similar between the post-reconstruction analysis and direct-4D reconstruction, especially in K_1 and blood volume. However, in Vd, TOF improvements are more noticeable in post-reconstruction analysis compared to direct 4D reconstruction owing to the reduced impact of emission/attenuation mismatch in the presence of inter-frame motion as mentioned above.

4. Discussion

Following many decades of hardware and software advancements, TOF PET imaging has now emerged as the standard method of data acquisition. The benefits stemming from its utilization originate in the constrained localization of annihilated events along their line-of-response with an accuracy depending on the scanner's TOF resolution. The main benefit of incorporating information about the photon arrival times within image reconstruction, is the apparent increase in the effective sensitivity resulting in an increase in the signal-to-noise ratio. The demonstrated gain depends mainly on patient's size, (randoms fraction) and TOF resolution and the resulted benefit can be used in static imaging to reduce the injected dose, reduce the scanned time or to improve image quality and subsequently lesion detectability. In dynamic imaging, similar performance gains can be used to increase temporal sampling rate or allow multi-bed dynamic imaging protocols. However, one side benefit of TOF imaging that has

received less attention is that TOF-based image reconstruction algorithms in static imaging are more robust in the presence of inconsistent correction data, such as attenuation, normalization and scatter as demonstrated first by (Conti 2011b). The underlying cause of this benefit is the same as the apparent SNR gain, in that any errors that originate in a point in space are not back-projected along the LOR traversing the entire FOV but only along a small segment, dictated by the system's timing uncertainty and represented by the TOF kernel. Such a benefit is critical in the presence of a less than optimum attenuation, as is the case in PET/MR (Mehranian and Zaidi 2015) or when normalization is only approximately accurate. In such cases, errors which would otherwise spatially propagate during back-projection, are kept more spatially localized or even minimized. Similar error propagation however occurs not only in static imaging but in dynamic imaging as well (Kotasidis *et al* 2011, 2012b). In the presence of inconsistent dynamic data/kinetic model, errors spatially propagate to other regions for which there is consistency between the model and the data. In this work, we investigated additional sources of errors that could arise in dynamic imaging, related to inter-frame bulk rigid-body motion. We hypothesized that using direct 4D image reconstruction for parameter estimation, inconsistencies between the dynamic data caused by activity blurring across frames and the kinetic model, could lead to errors temporally and spatially propagating to frames for which no motion occurs. Therefore, in the presence of such errors and taking advantage of the mechanics of TOF back-projection and its apparent benefits in static imaging, we investigated and demonstrated the benefit of TOF-based post-reconstruction and direct 4D image reconstruction techniques for kinetic parameter estimation.

Kinetic model induced bias has been demonstrated to exist when parameters are directly estimated within a 4D reconstruction algorithm, with adaptive models helping to minimize any errors in the TACs after the kinetic modelling step (Kotasidis *et al* 2014). However, a drawback identified is that such methods are as good as the selection of the secondary model used to capture any structure in the residuals. As such, it is unavoidable that noise will inevitably be captured as well, leading to its re-introduction back into the dynamic data. Therefore, there is a fine balance between reducing the kinetic model induced bias and increasing the noise induced bias and variance. On the other hand, inclusion of TOF appears to have no drawbacks and acts on limiting the propagation of bias at a stage where it already exists (during the tomographic step), as opposed to any adaptive model which attempts to limit its generation the first place (during the kinetic modelling step). However, as the results suggest, TOF alone although significantly reduces any propagation of bias, it doesn't completely eradicates it. Even at 160 ps, some bias still persisted in soft tissue around the heart ventricles. On the other hand, it was observed that bias reduction appears to be non-linearly related to the TOF resolution. Such a response can be attributed to the fact that there is a bias gradient, with errors being more pronounced closer to the erroneously modelled regions. Therefore, as TOF resolution improves, bias reduction becomes more pronounced. An improvement moving forward, would be the combination of TOF-based direct 4D algorithms with adaptive kinetic models, such as those proposed by (Matthews *et al* 2012, Germino *et al* 2015b). It is expected that the combination of both approaches for parameter estimation would minimize issues related to the application of a single model for the entire FOV. In this work, we focused on dynamic imaging in the body as opposed to applications in the brain. With the brain being significantly smaller compared to the torso, the influence of TOF on kinetic model induced errors is expected to be less noticeable and only at increased TOF resolutions. However, the limited influence of TOF is counterbalanced by the fact that such inconsistencies between the model and the data are less of a concern in dynamic brain imaging, since application of a common model throughout the brain is more feasible, with less diversity between the underlying kinetics.

Apart from inconsistencies due to diverse kinetics, we investigated potential error propagation from inter-frame body motion. The impact of emission/attenuation mismatch was investigated separately from inter-frame emission blurring and in combination. The reason is that attenuation related errors are not specific to dynamic imaging; therefore error propagation from them occurs not only in direct 4D methods but also in conventional 3D reconstruction, as the errors appear within each individually reconstructed frame. Therefore, in order to get a better understanding of the error propagation going from 3D to 4D parameter estimation, it was important to decompose the different sources of errors and evaluate their influence separately.

Directly reconstructed kinetic parameters were found to be only slightly more biased compared to those estimated from post-reconstruction analysis in the presence of emission/attenuation mismatch. This is probably due to the fact that attenuation errors occurring in the boundaries of regions, already spatially propagate within each individually reconstructed frame in 4D reconstruction (in the tomographic step and prior to the kinetic modelling step). Furthermore, to investigate attenuation mismatch alone, we simulated the case where the patient moved between the emission and transmission scans. Therefore, attenuation errors are similar across all frames, as opposed to the other 2 cases where we simulated patient motion between the 11th–21st frames and, as such, attenuation errors only appear in these frames. As errors and their propagation occur in all individually reconstructed frames, temporal propagation of these errors between frames during 4D reconstruction doesn't significantly add up to the already biased parameters seen in post-reconstruction analysis. This is in contrast to the case where inter-frame blurring was simulated alone, as when parameters are estimated post-reconstruction, errors are restricted solely on the boundaries of regions for which the TACs are blurred. This is to be expected since the activity was simulated to be constant within each region; therefore depending on the magnitude of motion, only a part of each region will experience activity blurring across frames. Although having a constant activity within each region is a simplification for computational purposes, it also makes it easier to identify any error propagation in direct 4D reconstruction. Error propagation appears to occur at two stages. First during the kinetic modelling step, the erroneous fit in the boundary regions will result in bias in the frames for which no motion occurs. Then similar to the kinetic model-induced and attenuation-induced errors, these errors will spatially propagate within each frame during the tomographic step of the 4D algorithm. It is then in this stage that TOF appears to help, as errors that already exist in the boundary regions, become more localized depending on the TOF resolution kernel.

Finally, when both the emission/attenuation mismatch and inter-frame activity blurring were considered together, additional error propagation was observed. However, the results suggested that the overall bias and its propagation is not just the summation of the individual biases. This could be explained by the fact that potential negative bias in a region due to attenuation mismatch could be partially negated by a positive bias due to inter-frame emission blurring. This would depend on the relative differences in activity and attenuation values between neighbouring regions as well as the magnitude and duration of motion. Nevertheless, in all individual or combined cases of the effects of inter-frame motion on kinetic parameters, TOF substantially reduced the propagation of errors both in 3D (attenuation errors) and 4D (attenuation + emission blurring errors) image reconstructions. However, in contrast to kinetic model induced errors, which are more pronounced in the body rather than the brain, inter-frame motion errors are a common source of errors in dynamic brain imaging. Due to the difference in size/diameter between the torso and the brain, inter-frame motion induced errors and their propagation are expected to benefit to a lesser degree when TOF-based image

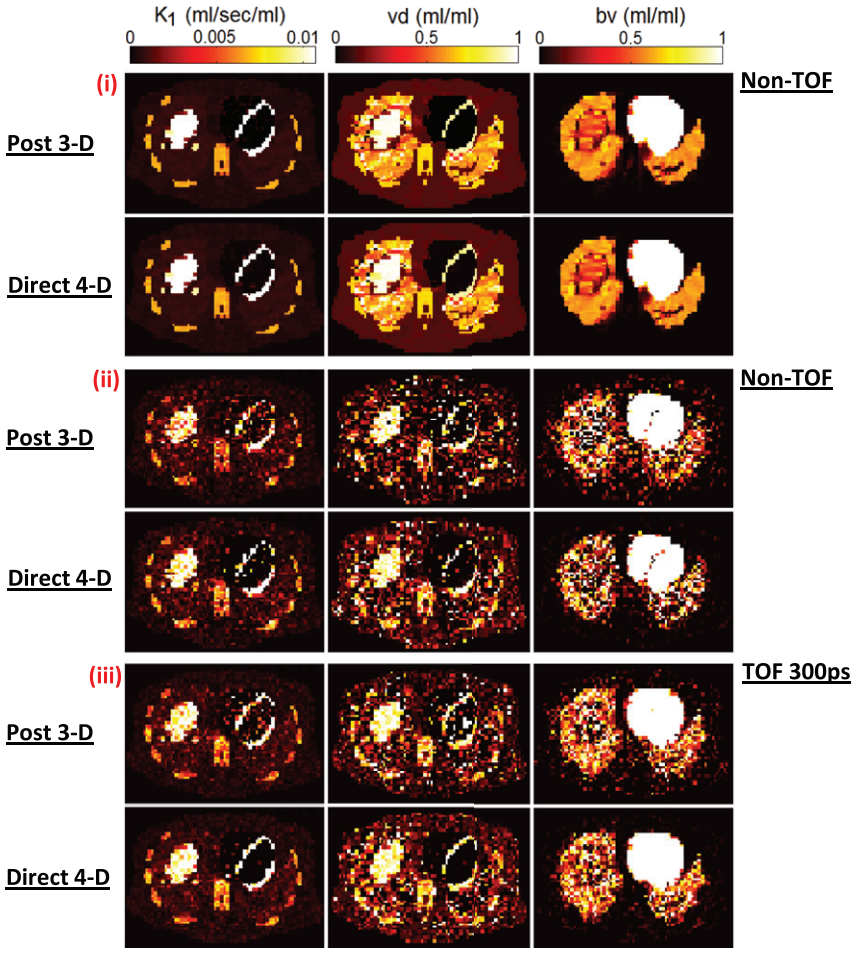

Figure 17. Estimated kinetic parameter maps without TOF for noiseless (i) and noisy (ii) data and with TOF (300 ps) for noisy data (iii). Parametric images are shown both for post-reconstruction kinetic analysis and direct 4D image reconstruction. Simulated data represent the ideal situation when no inconsistencies are present in the dynamic data. Under noiseless data, both post-reconstruction analysis and direct 4D give the same parameters (data shown at 8 iterations and 21 substers and have not fully converged comparing to the true parameters (figure 14(A-i)). Under noisy data and in the absence of inconsistencies, direct 4D reconstruction generated parametric maps with less variance compared to post-reconstruction analysis. The trend is the same whether TOF is used or not. Furthermore, comparing the non-TOF and TOF reconstructed data, the improvement in terms of SNR are also noticeable. Non-TOF and TOF images are compared at the same tumor-to-background contrast due to different convergence rates (non-TOF -(8 iterations and 21 substers); TOF −(2 iterations and 21 substers).

reconstruction algorithms are used for parameter estimation. Therefore, the benefits are only expected to be significant in higher TOF resolutions.

In all simulated inconsistencies investigated, post-reconstruction kinetic analysis consistently outperformed direct 4D image reconstruction in terms of bias. The reason is that compared to conventional post-reconstruction kinetic analysis, direct approaches to parameter estimation incorporate the temporal dimension within the reconstruction process. Therefore,

the temporal and the spatial dimension become interlinked and any errors occurring either during the tomographic, or the kinetic modelling step, will affect each other. Attenuation errors originate during the tomographic part and therefore errors can appear in the individually reconstructed time frames before the kinetic modelling step. On the other hand, errors due to inter-frame motion or erroneous modelling of the data occur in the temporal dimension and during the kinetic modelling step. Tomographic errors, such as attenuation, can propagate either spatially within each individual frame as in post-reconstruction analysis or propagate both spatially and temporally like in direct 4D reconstruction, with the kinetic model being the mean by which propagation occurs. On the other hand, errors originating in the kinetic modelling step, will only propagate in direct 4D reconstruction while in the post-reconstruction analysis such errors will be localized in the regions where the erroneous modelling occurred. As such, errors in direct 4D reconstruction will always be more severe than post-reconstruction analysis under inconsistent data. However, as elaborated in (Kotasidis *et al* 2014), bias can originate either from inconsistencies or from noise in the data. Bias in the kinetic parameters due to noise is far larger than bias due to inconsistencies. Therefore, under noisy data and given the noise-induced bias improvement of the direct 4D reconstruction against post-reconstruction analysis, the overall bias in the parameters directly estimated is still lower compared to parameters estimated indirectly, despite the additional bias due to propagation. In other words, the bias due to propagation is not sufficient to negate the noise-induced bias reduction that direct 4D methods offer compared to indirect 3D methods. Therefore, in this work we focused on using noiseless data and isolating the bias due to propagation, which limit the full benefit of direct parameter estimation methods, given the de facto superiority of direct 4D methods when noisy data are used. This is demonstrated in figure 17 where kinetic parameters were estimated using both noisy and noiseless data with no inconsistencies. As expected, under noiseless data both 3D and direct 4D reconstructions give similar parametric images with almost zero bias. Under noisy data, direct 4D substantially outperforms the post-reconstruction analysis.

Another motivation justifying the fact that we focused on noiseless data is that TOF not only limits bias due to propagation but also bias due to noise. As a consequence, adding noise would result in a bias reduction originating from both sources of bias, thus masking the benefits of TOF under inconsistent data alone. Finally, this study did not consider scatter or random events as the effect of these corrections on the kinetic parameters could potentially vary with the TOF resolution, thus masking the real impact of TOF on kinetic parameters in the presence of inconsistent dynamic data.

5. Conclusion

Time-of-flight image reconstruction algorithms are increasingly becoming the standard method for parameter estimation in PET imaging, whether to estimate activity concentrations or kinetic parameters. Apart from the obvious benefit of improving the SNR, TOF image reconstruction can prevent error propagation in the FOV, by limiting their spatial distribution, with a gain depending on the TOF kernel. This property can be used not only in static imaging applications but also in dynamic imaging as well, to prevent kinetic parameter error propagation both in 3D and direct 4D parametric image reconstruction. The propagation of errors induced by the inconsistencies between the data and kinetic model, could be significantly suppressed. Such improvements could facilitate the use of direct 4D reconstruction algorithms in dynamic abdominal and thoracic imaging for kinetic parameter estimation and allow their benefits to be fully exploited. Additional improvements could be further achieved by incorporating adaptive kinetic models within TOF-based parametric image reconstruction.

Acknowledgments

This work was supported by the Swiss National Science Foundation under Grant SNSF 31003A-149957.

References

Angelis G I, Matthews J C, Kotasidis F A, Markiewicz P J, Lionheart W R and Reader A J 2011 Evaluation of a direct 4D reconstruction method using GLLS for estimating parametric maps of micro-parameters *IEEE Nuclear Science Symp. and Medical Imaging Conf. (NSS/MIC), 2011* pp 2355–9

Anton-Rodriguez J M, Sibomana M, Walker M D, Huisman M C, Matthews J C, Feldmann M, Keller S H and Asselin M 2010 Investigation of motion induced errors in scatter correction for the HRRT brain scanner *IEEE Nuclear Science Symp. Conf. Record (NSS/MIC), 2010* pp 2935–40

Beyer T, Tellmann L, Nickel I and Pietrzyk U 2005 On the use of positioning aids to reduce misregistration in the head and neck in whole-body PET/CT studies *J. Nucl. Med.* **46** 596–602

Bloomfield P M, Spinks T J, Reed J, Schnorr L, Westrip A M, Livieratos L, Fulton R and Jones T 2003 The design and implementation of a motion correction scheme for neurological PET *Phys. Med. Biol.* **48** 959–78

Budinger T F 1983 Time-of-flight positron emission tomography: status relative to conventional PET *J. Nucl. Med.* **24** 73–8

Buerger C, Tsoumpas C, Aitken A, King A P, Schleyer P, Schulz V, Marsden P K and Schaeffter T 2012 Investigation of MR-based attenuation correction and motion compensation for hybrid PET/MR *IEEE Trans. Nucl. Sci.* **59** 1967–76

Conti M 2009 State of the art and challenges of time-of-flight PET *Phys. Med.* **25** 1–11

Conti M 2011a Focus on time-of-flight PET: the benefits of improved time resolution *Eur. J. Nucl. Med. Mol. Imaging* **38** 1147–57

Conti M 2011b Why is TOF PET reconstruction a more robust method in the presence of inconsistent data? *Phys. Med. Biol.* **56** 155–68

Conti M, Bendriem B, Casey M, Chen M, Kehren F, Michel C and Panin V 2005 First experimental results of time-of-flight reconstruction on an LSO PET scanner *Phys. Med. Biol.* **50** 4507–26

Conti M, Eriksson L and Westerwoudt V 2013 Estimating image quality for future generations of TOF PET scanners *IEEE Trans. Nucl. Sci.* **60** 87–94

Costes N, Dagher A, Larcher K, Evans A C, Collins D L and Reilhac A 2009 Motion correction of multi-frame PET data in neuroreceptor mapping: simulation based validation *Neuroimage* **47** 1496–505

Dinelle K, Ngo H, Blinder S, Vafai N, Topping G and Sossi V 2011 Frame-to-frame image realignment assessment tool for dynamic brain positron emission tomography *Med. Phys.* **38** 773–81

Feng D, Huang S C, ZhiZhong W and Dino H 1996 An unbiased parametric imaging algorithm for nonuniformly sampled biomedical system parameter estimation *IEEE Trans. Med. Imaging* **15** 512–8

Germino M, Sinusas A, Liu C and Carson R 2015a A hybrid kinetic model/B-spline algorithm for direct parametric reconstruction from cardiac list mode PET *Proc. Fully Three-Dimensional Image Reconstruction in Radiology and Nuclear Medicine*

Germino M, Sinusas A J, Liu C and Carson R E 2015b Assessment of kinetic modeling quality of fit by cluster analysis of residuals: application to direct reconstruction of cardiac PET data IEEE *Nuclear Science Symp. Conf. Record (NSS/MIC)* vol M6A1-5

Gravel P and Reader A J 2015 Direct 4D PET MLEM reconstruction of parametric images using the simplified reference tissue model with the basis function method for [(1)(1)C]raclopride *Phys. Med. Biol.* **60** 4533–49

Green M V, Seidel J, Stein S D, Tedder T E, Kempner K M, Kertzman C and Zeffiro T A 1994 Head movement in normal subjects during simulated PET brain imaging with and without head restraint *J. Nucl. Med.* **35** 1538–46

Häggström I, Schmidtlein C R, Karlsson M and Larsson A 2014 Compartment modeling of dynamic brain PET—the impact of scatter corrections on parameter errors *Med. Phys.* **41** 111907 (9pp)

Herzog H, Tellmann L, Fulton R, Stangier I, Rota Kops E, Bente K, Boy C, Hurlemann R and Pietrzyk U 2005 Motion artifact reduction on parametric PET images of neuroreceptor binding *J. Nucl. Med.* **46** 1059–65

Iida H, Higano S, Tomura N, Shishido F, Kanno I, Miura S, Murakami M, Takahashi K, Sasaki H and Uemura K 1988 Evaluation of regional differences of tracer appearance time in cerebral tissues using [15O] water and dynamic positron emission tomography *J. Cereb. Blood Flow Metab.* **8** 285–8

Iida H, Kanno I, Miura S, Murakami M, Takahashi K and Uemura K 1986 Error analysis of a quantitative cerebral blood flow measurement using H_2(15)O autoradiography and positron emission tomography, with respect to the dispersion of the input function *J. Cereb. Blood Flow Metab.* **6** 536–45

Jianhua Y, Planeta-Wilson B and Carson R E 2012 Direct 4D PET list mode parametric reconstruction with a novel EM algorithm *IEEE Trans. Med. Imaging* **31** 2213–23

Jiao J, Bousse A, Thielemans K, Markiewicz P, Burgos N, Atkinson D, Arridge S, Hutton B and Ourselin S 2014 *Medical Image Computing and Computer-Assisted Intervention—MICCAI 2014* ed P Golland *et al* (Berlin: Springer) pp 114–21

Jiao J, Searle G E, Schnabel J A and Gunn R N 2015 Impact of image-based motion correction on dopamine D3/D2 receptor occupancy—comparison of groupwise and frame-by-frame registration approaches *EJNMMI Phys.* **2** 15

Jin X, Mulnix T, Gallezot J-D and Carson R E 2013 Evaluation of motion correction methods in human brain PET imaging—a simulation study based on human motion data *Med. Phys.* **40** 102503

Kamasak M E, Bouman C A, Morris E D and Sauer K 2005 Direct reconstruction of kinetic parameter images from dynamic PET data *IEEE Trans. Med. Imaging* **24** 636–50

Keller S H, Sibomana M, Olesen O V, Svarer C, Holm S, Andersen F L and Højgaard L 2012 Methods for motion correction evaluation using 18F-FDG human brain scans on a high-resolution PET scanner *J. Nucl. Med.* **53** 495–504

Klein R, Hunter C, Beanlands R and deKemp R 2011 Prevalence of patient motion in dynamic PET *J. Nucl. Med.* **52** 2105

Konik A, Connolly C M, Johnson K L, Dasari P, Segars P W, Pretorius P H, Lindsay C, Dey J and King M A 2014 Digital anthropomorphic phantoms of non-rigid human respiratory and voluntary body motion for investigating motion correction in emission imaging *Phys. Med. Biol.* **59** 3669–82

Kotasidis F A, Matthews J C, Angelis G I, Markiewicz P J, Lionheart W R and Reader A J 2011 Impact of erroneous kinetic model formulation in direct 4D image reconstruction *Nuclear Science Symp. and Medical Imaging Conf. (NSS/MIC), 2011 IEEE* pp 2366–7

Kotasidis F A, Matthews J C, Reader A J, Angelis G I, Price P M and Zaidi H 2012a Direct parametric reconstruction for dynamic [^{18}F]-FDG PET/CT imaging in the body *IEEE Nuclear Science Symp. and Medical Imaging Conf. (NSS/MIC), 2012* pp 3383–6

Kotasidis F A, Matthews J C, Reader A J, Angelis G I and Zaidi H 2012b Application of adaptive kinetic modeling for bias propagation reduction in direct 4D image reconstruction *IEEE Nuclear Science Symp. and Med. Imaging Conf. (NSS/MIC), 2012* pp 3688–94

Kotasidis F A, Matthews J C, Reader A J, Angelis G I and Zaidi H 2014 Application of adaptive kinetic modelling for bias propagation reduction in direct 4D image reconstruction *Phys. Med. Biol.* **59** 6061–84

Kotasidis F A, Reader A J, Angelis G I, Markiewicz P J, Walker M D, Price P M, Lionheart W R and Matthews J C 2010 Direct parametric estimation of blood flow in abdominal PET/CT within an EM reconstruction framework *IEEE Nuclear Science Symp. Conf. Record (NSS/MIC), 2010* pp 2868–74

Kudomi N *et al* 2008 Non-invasive estimation of hepatic blood perfusion from H_2 ^{15}O PET images using tissue-derived arterial and portal input functions *Eur. J. Nucl. Med. Mol. Imaging* **35** 1899–911

Matthews J C, Angelis G I, Kotasidis F A, Markiewicz P J and Reader A J 2010 Direct reconstruction of parametric images using any spatiotemporal 4D image based model and maximum likelihood expectation maximisation *IEEE Nuclear Science Symp. Conf. Record (NSS/MIC), 2010* pp 2435–41

Matthews J C, Reader A J, Angelis G I, Price P M, Markiewicz P J and Kotasidis F A 2012 Adaptive parametric kinetic modelling for improved full field of view fitting of PET data *IEEE Nuclear Science Symp. and Medical Imaging Conf. (NSS/MIC), 2012* pp 3925–9

Mehranian A, Kotasidis F and Zaidi H 2016 Accelerated time-of-flight (TOF) PET image reconstruction using TOF bin subsetization and TOF weighting matrix pre-computation *Phys. Med. Biol.* **61** 1309–31

Mehranian A and Zaidi H 2015 Impact of time-of-flight PET on quantification errors in MR imaging-based attenuation correction *J. Nucl. Med.* **56** 635–41

Moses W W 2003 Time of flight in PET revisited *IEEE Trans. Nucl. Sci.* **50** 1325–30

Mourik J E, Lubberink M, Lammertsma A A and Boellaard R 2011 Image derived input functions: effects of motion on tracer kinetic analyses *Mol. Imaging Biol.* **13** 25–31
Mourik J M, Lubberink M, van Velden F P, Lammertsma A and Boellaard R 2009 Off-line motion correction methods for multi-frame PET data *Eur. J. Nucl. Med. Mol. Imaging* **36** 2002–13
Mukherjee J M, Johnson K L, McNamara J E and King M A 2010 Quantitative study of rigid-body and respiratory motion of patients undergoing stress and rest cardiac SPECT imaging *IEEE Trans. Nucl. Sci.* **57** 1105–15
Olesen O V, Paulsen R R, Hojgaard L, Roed B and Larsen R 2012 Motion tracking for medical imaging: a nonvisible structured light tracking approach *IEEE Trans. Med. Imaging* **31** 79–87
Qiao F, Pan T, Clark J W Jr and Mawlawi O R 2006 A motion-incorporated reconstruction method for gated PET studies *Phys. Med. Biol.* **51** 3769–83
Rahmim A *et al* 2008 Accurate event-driven motion compensation in high-resolution PET incorporating scattered and random events *IEEE Trans. Med. Imaging* **27** 1018–33
Rahmim A, Lodge M, Tang J, Zhou Y, Hussain B, Wong D, Pili R and Wahl R 2010 Dynamic FDG PET imaging using direct 4D parametric reconstruction in cancer patients *J. Nucl. Med.* **51** 354
Rahmim A, Rousset O and Zaidi H 2007 Strategies for motion tracking and correction in PET *PET Clin.* **2** 251–66
Rahmim A, Tang J and Mohy-ud-Din H 2014 Direct 4D parametric imaging in dynamic myocardial perfusion PET *Frontiers Biomed. Technol.* **1** 4–13
Rakvongthai Y, Ouyang J, Guerin B, Li Q, Alpert N M and El Fakhri G 2013 Direct reconstruction of cardiac PET kinetic parametric images using a preconditioned conjugate gradient approach *Med. Phys.* **40** 102501
Reader A J and Verhaeghe J 2014 4D image reconstruction for emission tomography *Phys. Med. Biol.* **59** R371–418
Surti S 2015 Update on time-of-flight PET imaging *J. Nucl. Med.* **56** 98–105
Surti S, Karp J S, Popescu L M, Daube-Witherspoon M E and Werner M 2006 Investigation of time-of-flight benefit for fully 3D PET *IEEE Trans. Med. Imaging* **25** 529–38
Tsoumpas C *et al* 2011 Fast generation of 4D PET-MR data from real dynamic MR acquisitions *Phys. Med. Biol.* **56** 6597–613
Wang G and Qi J 2009 Generalized algorithms for direct reconstruction of parametric images from dynamic PET data *IEEE Trans. Med. Imaging* **28** 1717–26
Wang G and Qi J 2012 An optimization transfer algorithm for nonlinear parametric image reconstruction from dynamic PET data *IEEE Trans. Med. Imaging* **31** 1977–88
Wardak M, Wong K-P, Shao W, Dahlbom M, Kepe V, Satyamurthy N, Small G W, Barrio J R and Huang S-C 2010 Movement correction method for human brain PET images: application to quantitative analysis of dynamic 18F-FDDNP scans *J. Nucl. Med.* **51** 210–8
Watabe H, Ikoma Y, Kimura Y, Naganawa M and Shidahara M 2006 PET kinetic analysis—compartmental model *Ann. Nucl. Med.* **20** 583–8
Westerwoudt V, Conti M and Eriksson L 2014 Advantages of improved time resolution for TOF PET at very low statistics *IEEE Trans. Nucl. Sci.* **61** 126–33
Ye H, Wong K P, Wardak M, Dahlbom M, Kepe V, Barrio J R, Nelson L D, Small G W and Huang S C 2014 Automated movement correction for dynamic PET/CT images: evaluation with phantom and patient data *PLoS One* **9** e103745